SENSING AND CONTROL OF ROTATING BLADE VIBRATIONS DUE TO THERMAL LOADS USING PIEZOELECTRIC MATERIALS

BY

AHMAD SHABAN OMAR

A Thesis Presented to the

DEANSHIP OF GRADUATE STUDIES

KING FAHD UNIVERSITY OF PETROLEUM & MINERALS

DHAHRAN, SAUDI ARABIA

In Partial Fulfillment of the
Requirements for the Degree of

MASTER OF SCIENCE

In

MECHANICAL ENGINEERING

MAY 2016

KING FAHD UNIVERSITY OF PETROLEUM & MINERALS

DHAHRAN- 31261, SAUDI ARABIA

DEANSHIP OF GRADUATE STUDIES

This thesis, written by AHMAD SHABAN OMAR under the direction of his thesis advisor and approved by his thesis committee, has been presented to and accepted by the Deanship of Graduate Studies, in partial fulfillment of the requirements for the degree of **MASTER OF SCIENCE IN MECHANICAL ENGINEERING**.

Dr. Mehmet Sunar
(Advisor)

Dr. Zuhair Gasem
Department Chairman

Dr. Husain M Al-Qahtani
(Member)

Dr. Salam A. Zummo
Dean of Graduate Studies

Dr. Khaled Al-Athel
(Member)

29/5/16

Date

May 2016

To my Beloved

Parents, Brother, and Sisters

ACKNOWLEDGMENTS

"In the name of Allah, the Most Beneficent and Most Merciful"

First of all, I would like to thank almighty Allah for this achievement. He provided me with his blessings throughout all my life and gave me the health, patience and strength to reach this level of knowledge and accomplish this work. I pray to almighty Allah to make this thesis beneficial knowledge "on the day when neither wealth nor sons shall benefit anyone, except for him who comes before Allah with a pure heart".

I would like to thank my parents and my distinguished instructors who helped me understand that Allah taught man what he did not know, that a scientist meets his end while still lacking knowledge, and that modesty only adds to a scientist' sublimity.

Special thanks go to my beloved father and mother who have always had faith in me, and for their patience and love. They have always helped and provided me all the unconditional support that I needed over the years in school and college. Thanks also go to the rest of my family, especially my brother and sisters, who encouraged me and gave me their love and affection.

I would like to express my sincere gratitude to my thesis advisor Dr. Mehmet Sunar for his continuous guidance and efforts throughout my Master's graduate program. He helped me a lot in my Master's thesis, and taught me many things in the area of Finite Element Method and System Dynamics & Control. In addition, I learned a lot from him in both morals and science.

Special thanks and deep appreciation is extended to Dr. Husain Al-Qahtani and Dr. Khaled Al-Athel, for their generous help, encouragement, and being part of my evaluation committee in my graduate program.

I would like also to thank all my friends and colleagues who supported or helped me whether in my life or academic career.

May Allah raise degrees of my parents and my distinguished teachers, and grant them all health, wellness and long lives.

To them all, I dedicate this work.

TABLE OF CONTENTS

LIST OF TABLES

LIST OF FIGURES

ABSTRACT

Full Name : Ahmad Shaban Omar

Thesis Title : Sensing and Control of Rotating Blade Vibrations due to Thermal Loads using Piezoelectric Materials

Major Field : Mechanical Engineering

Date of Degree : May 2016

Vibration sensing and control of rotating beams using piezoelectric materials subjected to thermal loads are considered in this thesis. Thermal loads are important in many applications such as turbo-machinery, where thermal effects should be imposed on rotating blades/beams in addition to other mechanical effects. Thermal effects are imposed on turbine blades, which are assumed to be mounted with piezoelectric patches for vibration sensing and control. Effects of the temperature field on the piezoelectric media are treated through the phenomenon of thermopiezoelectricity where electrical, mechanical, and thermal fields are all coupled. First, static beams/plates are considered without control in order to analyze temperature distribution for a beam along its thickness due to a uniform heat flux, followed by the lateral vibrations of the beam caused by the temperature gradients; using the finite element method and analytical equations for comparison purposes. The well-known finite element package ANSYS is utilized to implement the finite element method in all cases. The analytically and finite element approaches for both the temperature distribution and lateral vibrations of the beam have resulted in almost identical solutions. After that, the rotating blades bonded with piezoelectric materials are then analyzed for sensing and control of thermally-induced vibrations. The attenuation of rotating blade responses (vibrations) due to thermal loads are investigated through an appropriate control laws. Resulting voltages are confined to a maximum voltage of 500 V per mm of the PZT layer thickness and temperatures to values much less than the Curie point of 365oC for proper functioning of piezoelectric elements.

MASTER OF SCIENCE DEGREE
KING FAHD UNIVERSITY OF PETROLEUM AND MINERALS
Dhahran, Saudi Arabia

ملخص الرسالة

الاسم الكامل : أحمد شعبان عمر

عنوان الرسالة : الاستشعار والتحكم باهتزازات العوارض الدوارة تحت تأثير عبء حراري بإستخدام المواد ذات الكهرباء الإجهادية

التخصص : الهندسة الميكانيكية

تاريخ الدرجة العلمية : شعبان 1437هـ

سوف يتم التركيز على استشعار الاهتزازات والتحكم بالعوارض الدوارة بإستخدام المواد ذات الكهرباء الإجهادية تحت تأثير عبء حراري في هذه الدراسة. في البداية، ستتم دراسة وتحليل اهتزازت العورارض الثابتة المستحثة حراريًا، حيث سيتم تطبيق العبء الحراري على طول العارضة مما سيؤدي إلى اهتزازات جانبية بسبب تغيير الحرارة مع الوقت. سيتم دراسة وحساب انتشار وتوزيع كل من الحرارة والإزاحة في العارضة عن طريق المعادلات التحليلية وبإستخدام طرق العناصر المنتهية. المعادلات التحليلية ستكون مبنية على توظيف نظرية التوصيل الحراري ونظرية "داليمبيرت" لحساب انتشار وتوزيع الحرارة والإزاحة المرتبطين بتغير الوقت. ستتم الإستفادة من طريق العناصر المنتهية لحساب نفس النتائج عن طريق التحليل الحراري والإنشائي الوقتي. ستتم مقارنة النتائج المستخرجة عن طريق الأساليب التحليلية وطرق العناصر المنتهية ببعض لغرض التأكد من صحتها. سيتم استخدام برنامج طرق العناصر المنتهية المعروف بـANSYS لدراسة وتحليل الاهتزازات المستحثة حراريًا لعارضة دوارة .النتائج المستخرجة عن طريق الأساليب التحليلية وطرق العناصر المنتهية لكل من الحرارة والإزاحة في العارضة متطابقة تقريبًا .سيتم فرض اهتزازات العارضة الجانبية على المادة ذات الكهرباء الإجهادية الملتصقة بالعارضة للإستشعار بالاهتزازات والتحكم بها في الجزء الثاني من هذه الدراسة، سيتم استشعار اهتزازات العرضة الدوارة والتحكم بها أيضًا باستخدام طبقة من المواد ذات الإجهادية مرتبطة بسطح العارضة الدوارة. سيتم دراسة وفحص تخفيف الاهتزازات في العارضة الثابتة والعارضة الدوارة تحت تأثير عبء حراري سيتم عن طريق قوانين تحكم مناسبة وملائمة. النتائج المستخرجة عن طريق طرق العناصر المنتهية أوجدت أن فرق الجهد الناتج مقتصر على 500 فولت لكل ملم من سمك طبقة المواد ذات الكهرباء الإجهادية إضافة إلى درجات حرارة أقل بكثير من 365 درجة مئوية وهي درجة الحرارة المتسببة في تغيير خصائص المواد ذات الكهرباء الإجهادية حيث تصبح غير صالحة بعدها وهذا ما كان يجب البرهنة عليه.

درجة الماجستير في العلوم
جامعة الملك فهد للبترول والمعادن
الظهران، المملكة العربية السعودية

CHAPTER 1

INTRODUCTION

Thermal analysis for temperatures, stresses, and/or displacements has always been a focus of interest in scientific communities due to involvement of thermal field in vastly different areas [1]. In particular to thermally-induced vibrations, some examples include applications of high temperatures and heat in turbo machinery to produce power.

Beams are basic, but important structural elements, because many systems can be simply modeled as such. Hence, they have been the subject of many investigations in various mechanical and structural studies; a robot arm, a turbine blade, and an airplane wing can be modeled as a beam, to name a few [2].

Thermopiezoelectric or piezothermoelastic materials can be used in vibration sensing and control because of the thermopiezoelectric phenomenon, which couples thermal, mechanical, and electrical fields together. Hence, these materials have found many applications in robotics, aerospace, turbomachinery, microelectromechanical systems (MEMS), etc. [3].

The finite element method (FEM) is a robust numerical approach used in the analysis of many modern systems. It divides a system into small parts, called finite elements, and then assembles them to solve for temperatures, displacements. etc., on the

global system. The solution is then post-processed to obtain dependent variables such as strains and stresses.

1.1 LITERATURE REVIEW

In 1880, two French physicist brothers, Jacques and Pierre Curie were the first who discovered the piezoelectric effect [4], [5]. Piezoelectricity basically defines a relationship between electric and mechanical stress/strain fields in certain materials [6]. Specially shaped crystals of natural minerals, quartz in particular, were originally used. Nowadays, there are several piezoelectric materials used in various applications including: Lead Zirconate Titanate (PZT), Aluminum Nitride (AIN), Zinc Oxide (ZnO), Quartz (SiO2), Poly-Vinylidene Fluoride (PVDF) and others [7]. The manufactured ceramics are the most commonly used piezoelectric materials such as Ceramic B, PZT-2, PZT-4, PZT-5A, PZT-5H, etc., due to their special characteristics, and the piezoelectric materials. The piezoceramics are used as either sensors or actuators [8].

Adaptive structures using piezoelectric materials are usually called smart structures. The piezoelectric materials have been utilized extensively in precision control of dynamical systems. Using piezoelectric materials in active control applications has proved that they are very good in sensing and controlling to reduce vibration and counteract any undesired disturbance.

Thermally induced vibrations of internally heated beams were analyzed by Murozono [9]. Theoretical and experimental results were obtained and compared. Composite beams with interlayer slip operating under thermal loads were examined by Adam et al [10]. The resulting boundary value problem was solved using a mixed closed

form and truncated modal series procedure for the quasi-static and complementary dynamic portions. Structural vibrations due to thermal loads were controlled via piezoelectric pulses by Tauchert and Ashida [11]. Al-Bedoor et al [12] developed a technique for blade vibration measurements in turbo-machinery and jet engines.

Active vibration control of a cantilever beam with a pair of piezoceramic patches was considered by Vasques and Rodrigues [13] where they analyzed velocity response of the beam to a harmonic excitation and an initial displacement field. Sunar and Al-Bedoor [2] investigated the usability of a piezoceramic (PZT) sensor placed in the root of a stationary cantilever beam for measuring structural vibrations during both the transient and steady-state phases.

In another study, free and forced vibration of a laminated variable thickness FGM Timoshenko beam under heat effects was investigated by Xiang and Yang [14]. The beam was imposed upon one dimensional steady heat in its thickness direction and Lagrange interpolation polynomials were utilized as a numerical tool to solve the resulting thermo elastic and dynamic equations. Dynamical response of a cylindrical rod subjected to a non-uniform heat was analyzed by Bertarelli et al [15] through analytical and experimental means. The applied heat causes fast temperature increase in the rod producing longitudinal and flexural vibrations in return. A lightweight piezocomposite actuator was used by Suhariyono et al [16] to attenuate vibrations of a cantilever aluminum beam. A digital PID control process was implemented in the active vibration suppression system.

The study of a cantilever beam with a piezoceramic actuator and sensor through a pole placement control of multimodal vibration suppression was presented by Sethi and Song [17]. The spectral element model for the axially moving plates subjected to thermal loadings was developed by Lee and Kwon [18]. Numerical results revealed that dynamic response of the spectral element model for an axially moving uniform plate neglecting its length and considering the plate as one finite element component was very accurate. Vibration and stability studies of a composite beam under thermal and magnetic fields were undertaken by Wu [19] where various results including those displaying phenomena of beats and resonance were shown.

Formulation for analyzing piezothermoelastic fibers compound shell design with attested actuators and piezoelectric sensors was developed by Roy et al developed [20]. A simply-supported beam subjected to step heat input, sudden heating and dynamic stresses was studied by Marakala et al [21]. They used the finite element method for the solution to thermally induced vibrations. They found out that the displacement increases while the frequency of oscillation decreases. Displacement control of a compound cylinder comprising of a thermoelastic inner layer in touch with the outer layer was considered by Tauchert and Howard [22]. Voltage was applied to the outer surface of the cylinder in order to repress the thermally-induced radial displacement.

An Euler-Bernoulli beam of large rotation was analyzed by Shen et al [23] for the coupled effects of thermal and structural loads. Thermally induced vibration of a cantilever beam was studied by Kidawa-Kukla [24] with an assumption of the surface of the beam acting as a periodically time-varying heat source. Thermal stresses produced by the changing of the beam temperature led to displacements in the beam.

Thermal impact on dynamics of a damped cantilever Timoshenko beam of temperature-dependent elastic modulus was analyzed theoretically by Gu et al [25]. Temperature gradient induced thermal force that helped to determine the thermal effect.

Malgaca et al studied the control behaviors of rotating blades vibrations through piezoelectric materials at the root [26]. Smart materials were used by Kerboua et al [27] to reduce and control the vibration of cantilever beams. Optimal design and location of piezoelectric transducers were studied by applying the finite element method. Romaszko et al [28] analyzed forced vibrations of a homogeneous cantilever beam subjected to kinematic excitation with a moving holder via the application of a vision method.

1.2 OBJECTIVES

The main objective of this thesis is the sensing and control of thermally generated responses of stationary and rotating beams by the use of piezoelectric materials. This study is important for mechanical/structural elements subjected to heat loads that cannot be ignored. These heat inputs alone may result in thermally induced vibrations or may add up to already existing mechanical vibrations from other sources. Monitoring and controlling vibrations due to thermal and other effects are very important for the safe functioning of industrial systems operating under various disturbances.

1.3 LAYOUT OF THESIS

In the first part of this thesis in chapter 2, simply supported and cantilever stationary blades (beams/plates) are subjected to the step load of uniform heat, resulting in time varying temperature and displacement fields in the blade. Temperature and lateral displacement fields are computed analytically then by finite element methods. Analytical and finite element results are analyzed and compared with each other for verification. Lateral displacements of the blade are then sensed and controlled by piezoelectric materials bonded to the beam through a feedback control scheme.

In the second part of the thesis in chapters 3 and chapter 4, the cantilever blade mounted with piezoelectric materials is given rotation and then the rotating system is considered for thermally induced vibration sensing and control. The feedback controller designed for the stationary blade is used for the rotating blade control with some feedback gain modifications.

CHAPTER 2

THERMALLY-INDUCED VIBRATION ANALYSIS FOR STATIONARY BLADES

In this chapter, analytical solution of Fourier heat conduction equation given below is presented and solved for temperature distribution in a beam (blade) due to a thermal load. The resulting temperature distribution is used to obtain lateral displacements of the beam by employing the beam deflection equation provided in the following section. The same beam is also modeled by ANSYS finite element program via transient thermal analysis and solved for temperature, which is utilized through transient structural analysis to obtain lateral displacements of the beam. The analytical and finite element results are then assessed and compared with each other.

2.1 Analytical Method

2.1.1 Temperature Distribution

The heat conduction is one of three modes by which the heat transfer occurs. For an isotropic solid, the heat conduction or diffusion equation is given by [29]:

$$k(\nabla^2 T) + Q = (\rho c)\frac{\partial T}{\partial t} + (\rho c)\frac{\partial (uT)}{\partial x} \tag{2.1}$$

where:

k: thermal conductivity (W/mK),

∇^2: The gradient vector,

T: Solid temperature (K),

Q: Heat input rate per unit volume (W/m^3),

ρ: Material density (kg/m^3),

c: Specific heat (J/kg.K), and

t: time (sec).

Equation 2.1 is solved to determine the beam temperature T for various initial and boundary conditions. The initial conditions specify the initial temperature distribution of the beam, which is taken to be constant for most problems at time zero, i.e. $T(x,0) = T_\infty$, where, T_∞ is the free air stream temperature caused by the beam. As for the boundary conditions, there are several cases, one of which is the surface insulation. This case requires that there is no heat flux, i.e. q_h=0, across the insulated surface along a direction of x. This is mathematically expressed as $\frac{\partial T}{\partial x} = 0$. While in other cases, there is a presence of convective heat transfer, i.e. $q_h = h_c(T - T_\infty)$, where h_c is the convective heat transfer coefficient. This is shown through substituting in the heat conduction law:

$$q_h = -k\frac{\partial T}{\partial x} \tag{2.2}$$

By using linear Lagrange interpolation function, the finite element equation for temperature distribution upon the thickness of the plate when the beam is under effect of sudden heating on one side and insulated on other surface is as follows [30]:

$$\frac{kA}{l}\begin{bmatrix} 1 & -1 \\ -1 & 1 \end{bmatrix}\begin{Bmatrix} T_1 \\ T_2 \end{Bmatrix} + \frac{\rho cAl}{6}\begin{bmatrix} 2 & 1 \\ 1 & 2 \end{bmatrix}\begin{Bmatrix} \dot{T}_1 \\ \dot{T}_2 \end{Bmatrix} = \frac{\dot{q}Al}{2}\begin{Bmatrix} 1 \\ 1 \end{Bmatrix} \tag{2.3}$$

However, for the plate affected by sudden heating on one surface and naturally uniform convection on the other sides of the beam is given by

$$\left\{\frac{kA}{l}\begin{bmatrix}1 & -1\\ -1 & 1\end{bmatrix}+\begin{bmatrix}0 & 0\\ 0 & h_cA\end{bmatrix}\right\}\begin{Bmatrix}T_1\\ T_2\end{Bmatrix}+\frac{\rho cAl}{6}\begin{bmatrix}2 & 1\\ 1 & 2\end{bmatrix}\begin{Bmatrix}\dot{T}_1\\ \dot{T}_2\end{Bmatrix} = \frac{\dot{q}Al}{2}\begin{Bmatrix}1\\ 1\end{Bmatrix}+h_cAT_\infty\begin{Bmatrix}0\\ 1\end{Bmatrix} \tag{2.4}$$

where T_1 and T_2 are the nodal temperatures and T_∞ is the ambient temperature. The 2nd vector on the right hand side and 2nd matrix on the left hand side are contributed by convection and will be taken into consideration for the last element only.

The global finite element equation for time dependent temperature distribution has the following form:

$$\mathrm{K}^{\mathrm{e}}_{\mathrm{comb}}T+\mathrm{K}^{\mathrm{e}}_{\mathrm{cap}}\dot{T}=\bar{\mathrm{F}}^{\mathrm{e}}_{\mathrm{Q}} \tag{2.5}$$

where $\mathrm{K}^{\mathrm{e}}_{\mathrm{comb}}$ is the convection matrix, $\mathrm{K}^{\mathrm{e}}_{\mathrm{cap}}$ is the element capacitance matrix, and $\bar{\mathrm{F}}^{\mathrm{e}}_{\mathrm{Q}}$ is the force vector. Equation 2.5 must be solved for the variation of temperature in time domains and space to obtain the temperature distribution which can be calculated and solved using the method of finite central difference [31].

The closed form solution for the temperature distribution of the beam is given by [32]

$$T(y,\tau) = \frac{hQ}{k}\left\{\tau + \frac{1}{2}\left(\frac{y}{h}+\frac{1}{2}\right)^2 - \frac{1}{6} - \frac{2}{\pi^2}\sum_{j=1}^{\infty}\frac{(-1)^j e^{-j^2\pi^2\tau}}{j^2} cos\, j\pi\left(\frac{y}{h}+\frac{1}{2}\right)\right\} \tag{2.6}$$

where y is the vertical distance from the neutral axis of the beam, h is thickness of the beam, and τ is a non-dimensional time parameter defined by:

$$\tau = \frac{\kappa t}{h^2} \tag{2.7}$$

The thermal diffusivity κ is given by

$$\kappa = \frac{k}{\rho c} \tag{2.8}$$

2.1.2 Thermally-Induced Vibrations of Beams Subjected to External Heat Source

Consider a differential element *dx*, of a thin beam under the action of external forces and thermal loads. T_t and T_b correspond to the temperature on the top and bottom surfaces respectively, while F is the shear force and p is the load intensity. The stationary beam is assumed to be an isotropic solid with a uniform cross-section lying in the x direction. According to [33] the curvature of a uniform beam under the simultaneous actions of applied loads and Euler–Bernoulli's heat input can be expressed as:

$$M + M_T = EI\left(\frac{\partial^2 v}{\partial x^2}\right) \tag{2.9}$$

where M is the internal bending moment, M_T is the thermal moment which is due to temperature gradient across the thickness of the beam, I is the moment of inertia of the beam cross section, and v is the lateral displacement in the x direction.

The thermal moment acts as a forcing function for the beam exposed to heat flux on one surface and insulated on the other sides is given as

$$M_T = \int_A E \cdot \alpha \cdot \Delta T \cdot z \cdot dA \tag{2.10}$$

where ΔT is the change in the temperature.

The total thermal moment across the section is found by calculating and summing up the thermal moment at uniform intervals from the top to bottom surfaces of the beam. There is no temperature variation along the length of the beam, which means that the temperature is independent of x, hence, $M_T = M_T(t)$.

Differentiating of equation 2.9 twice with respect to x, the resulting expression is

$$\frac{\partial^2 M}{\partial x^2} + \frac{\partial^2 M_T}{\partial x^2} = \frac{\partial^2}{\partial x^2}\left(EI\frac{\partial^2 v}{\partial x^2}\right) \tag{2.11}$$

According to D'Alembert's principle the applied loads will be equated to the negative of the inertia force as follows:

$$\frac{\partial^2 M}{\partial x^2} = -\rho A\left(\frac{\partial^2 v}{\partial t^2}\right) \tag{2.12}$$

where ρ is the density of the beam, and A is the cross sectional area.

Using equation 2.12 in equation 2.11 will yield in the governing equation for lateral displacement (deflection) of a beam in the transverse direction in the presence of thermal moment as

$$\frac{\partial^2 M_T}{\partial x^2} = EI\frac{\partial^4 v}{\partial x^4} + \rho A\frac{\partial^2 v}{\partial t^2} \tag{2.13}$$

For vibrations due to the above thermal load, the stationary beam is assumed to be an isotropic solid with a uniform cross-section lying in the x direction. Hence, the governing equation for the lateral beam displacement v is expressed as [34]:

$$(EI)\frac{\partial^4 v}{\partial x^4} + (\rho A)\frac{\partial^2 v}{\partial t^2} = \frac{\partial^2 M}{\partial x^2} \tag{2.14}$$

where E is the beam's modulus of elasticity, I is second area-moment, A is cross-sectional area, ρ is mass density, and M is moment caused by thermal effects generated within the beam.

The solution of this equation again requires initial and boundary conditions for the displacement field. The beam is considered to be initially at rest with simply supported boundary condition for the previous analytical study. The non-dimensional thermal moment is given by

$$m(\xi, \tau) = \frac{\pi^4 kM}{192QEI\alpha} \tag{2.15}$$

where α is thermal expansion coefficient, and the non-dimensional parameter ξ is defined as the ratio of variable x to length of the beam L

$$\xi = \frac{x}{L} \tag{2.16}$$

The non-dimensional lateral deflection V is defined in terms of physical lateral deflection v by

$$V(\xi, \tau) = \frac{\pi^4 k v}{192 Q \alpha L^2} \tag{2.17}$$

Another non-dimensional parameter B is introduced as

$$B = \frac{h}{L\sqrt{\kappa}} \left(\frac{EI}{\rho A}\right)^{1/4} \tag{2.18}$$

where h is the height or thickness of the rectangular beam.

The non-dimensional lateral deflection is then found as

$$V = V_{st} - \sum_{n=1,3,5}^{\infty} \frac{\sin n\pi\xi}{n^3\pi^3} \left[\frac{\pi^2}{8B^2n^2} \sin n^2\pi^2B^2\tau - \sum_{j=1,3,5}^{\infty} \frac{e^{-j^2\pi^2\tau} + (j/nB)^2 \sin n^2\pi^2B^2\tau - \cos n^2\pi^2B^2\tau}{j^4 + n^4B^4} \right] \tag{2.19}$$

where V_{st} is the static non-dimensional deflection solution given by

$$V_{st}(\xi, \tau) = -\frac{m_T}{2}(\xi^2 - \xi) \tag{2.20}$$

2.1.3 Damping Ratio

It is sometimes important to determine the damping ratio and damped natural frequency f_n of systems. To determine the damping ratio of a system, a damped oscillation is needed, as shown in Figure 2.1 [35].

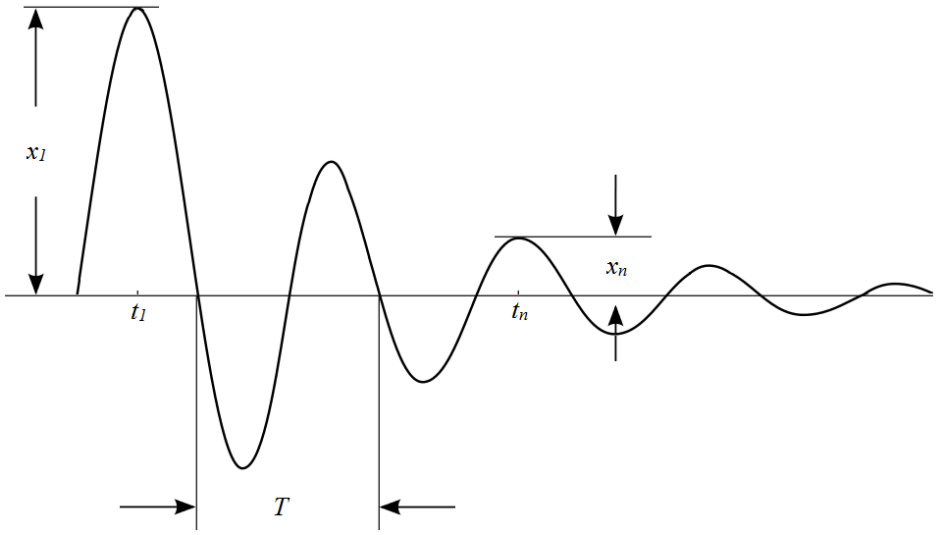

Figure 2.1: Decaying oscillation.

The fundamental natural frequency f_n in Hz is given as

$$f_n = \frac{1}{2\pi}\left(1.875^2\sqrt{\frac{EI}{\rho AL^4}}\right) \tag{2.21}$$

To find the damping ratio ζ we measure amplitudes from the rate of decay of the oscillation. Therefore, at time $t = t_1$ we calculate the amplitude x_1, and at $t = t_1 + (n - 1)T$, we calculate the amplitude x_n, where T is the period of oscillation.

We obtain the equation (2.22) below, by having the ratio of the exponential multiplying factors at t_1 and $t_1 + T$ (representing the decay in amplitude from one cycle to the next cycle),

$$\frac{x_1}{x_n} = \frac{1}{e^{-\zeta\omega_n(n-1)}} = e^{(n-1)\zeta\omega_n} \tag{2.22}$$

The logarithmic decrement which is the logarithm of the ratio succeeding amplitudes can be obtained by:

$$\frac{1}{n-1}\left(\ln\frac{x_1}{x_2}\right) = \frac{2\pi\zeta}{\sqrt{1-\zeta^2}} \tag{2.23}$$

Thus, the damping ratio ζ is found from

$$\zeta = \frac{\frac{1}{n-1}\left(\ln\frac{x_1}{x_2}\right)}{\sqrt{4\pi^2 + \left[\frac{1}{n-1}\left(\ln\frac{x_1}{x_2}\right)\right]^2}} \tag{2.24}$$

2.2 Thermally-Induced Vibration Analysis for Stationary Blades Modeling

This section presents models of both the simply-supported and cantilever blades (beams) that are subjected to the step load of uniform heat, resulting in time varying temperature and displacement fields in the blade. The mathematical model discussed in Section 2.1 is coded into a computer program using MATLAB. The beam is simulated using the finite element program ANSYS.

2.2.1 Case 1: Simply-Supported Beam

In this section, a simply-supported uniform rectangular aluminum beam of length L, width b and height h as shown in Figure 2.2 is tested for temperature distribution and lateral displacement. A uniform step heat flux of $Q = 1.5\times10^7$ W/m^2 is applied on the top surface over the edge $y = (h/2)$, and the other surfaces are insulated.

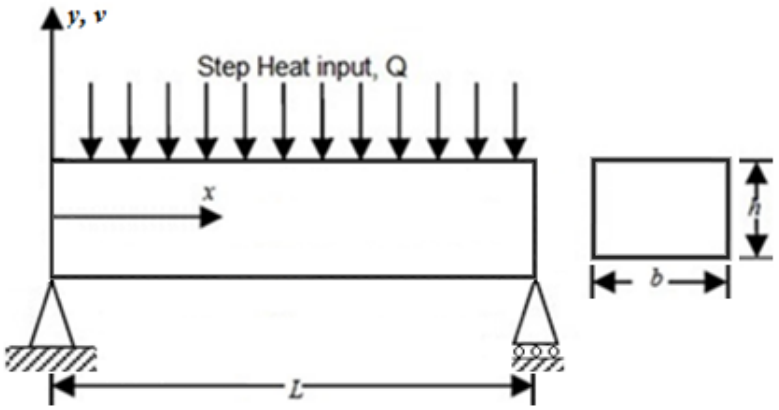

Figure 2.2: Simply-supported rectangular beam subjected to uniform step heat input.

The length of the beam is taken as $L = 0.254$ m. But, the width and thickness (height) of the beam are taken such that two values of parameter B are defined in

equation (2.18) in order to compare the finite element results with the analytical ones as in [34]. In one case, the value of B=1 is obtained when the width and height of the beam are taken as b=0.0052 m and height h=0.0015686 m, respectively. In the other case, the value of B is assumed to be very large (B=∞). The material properties of aluminum beam are listed in Table 2.1.

We tested the beam using ANSYS to solve for temperature distribution followed by structural response as shown in Figure 2.3 and Figure 2.4. We used two cases to model the beam: in the first, we investigated the finite element's solid type that used the "PLANE183" element type where thermal and structural fields are both coupled; whereas in the second case, we used element types "SHELL131" and "SHELL181" which represent the thermal field and the structural field, respectively, in order to find the finite element's shell solution.

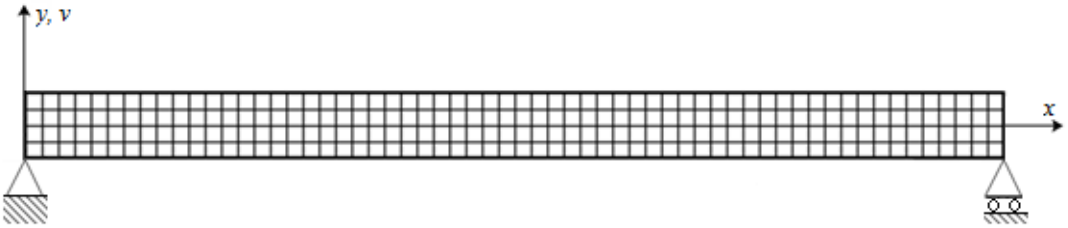

Figure 2.3: Finite element model for simply supported beam (not to scale).

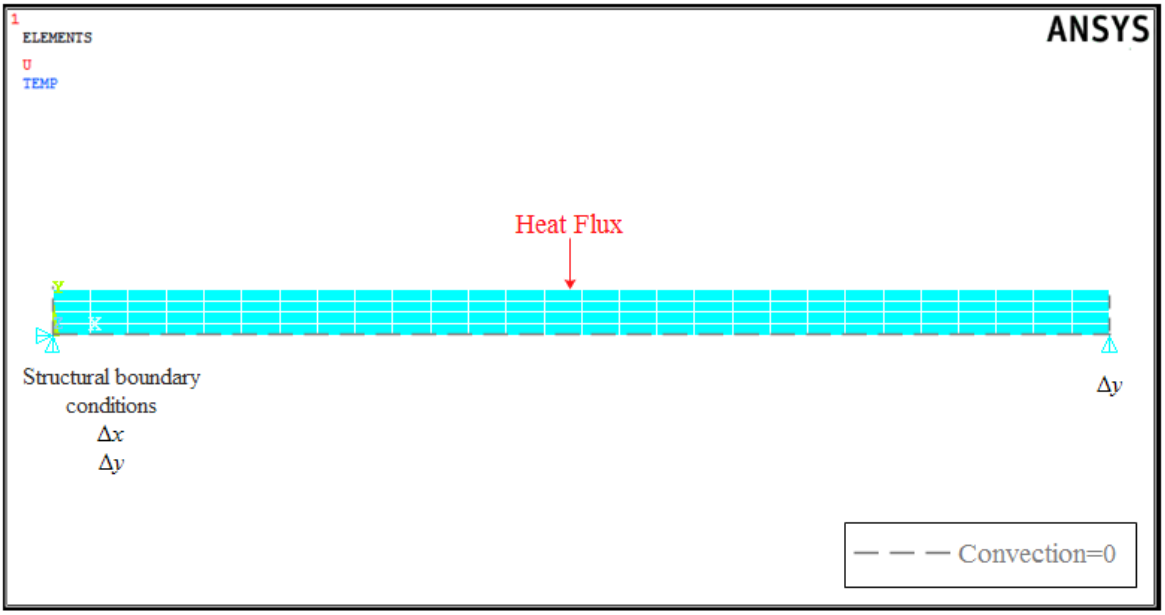

Figure 2.4: Finite element model for simply supported beam in ANSYS.

Table 2.1: Material properties for aluminum beam.

Thermal expansion coefficient α (1/K)	22.2×10^{-6}
Conductivity k (W/mK)	210
Specific heat c (J/kg·K)	904.5
Density ρ (kg/m^3)	2700
Modulus of Elasticity E (Pa)	7×10^{10}
Poisson's ratio ν	0.33

2.2.2 Case 2: Cantilever Beam

In this case, a steel cantilever beam (Figure 2.5) is subjected to step uniform heat flux input of $Q = 1.5\times10^7$ W/m^2 and is tested for temperature distribution and lateral displacement. The heat input Q is applied on the top surface ($y=h/2$) of the beam, while the other sides are insulated (convection = 0). The length, width and thickness of the beam are taken as L=0.122 m, b=0.0254 m and h=0.001 m, respectively. Material properties of the steel beam are listed in Table 2.2.

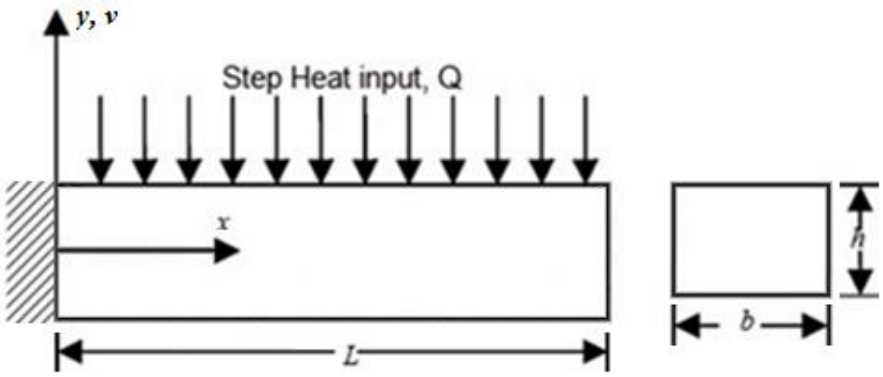

Figure 2.5: Cantilever beam subjected to uniform step heat input.

In ANSYS, the cantilever beam is modeled by the structural shell (SHELL181) and thermal shell (SHELL131) element for the thermal analysis followed by the structural analysis, and is meshed into 180 elements as shown in Figure 2.6 and Figure 2.7.

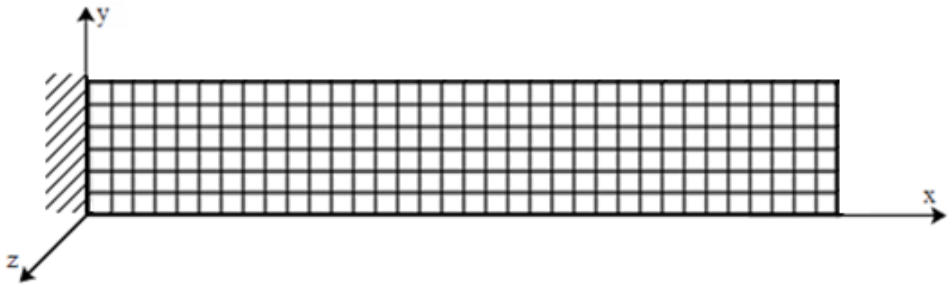

Figure 2.6: Finite element model for cantilever shell (not to scale).

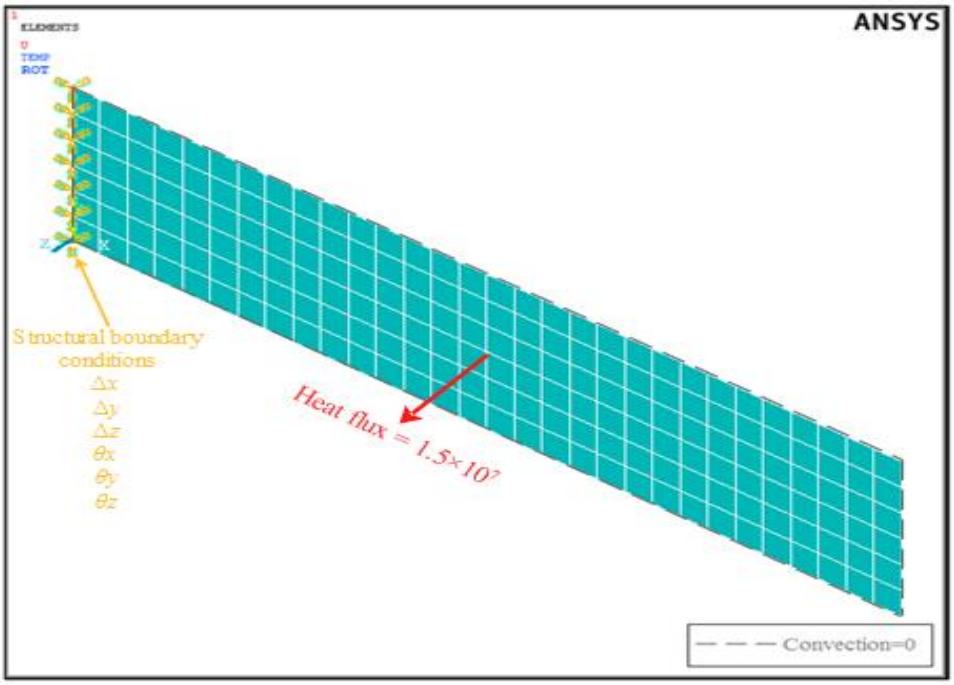

Figure 2.7: Finite element model for the cantilever shell in ANSYS.

Table 2.2: Material properties for steel beam.

Thermal expansion coefficient α (1/K)	10.8×10^{-6}
Conductivity k (W/mK)	43
Specific heat c (J/kg.K)	490
Density ρ (kg/m^3)	7800
Young's modulus E (Pa)	207×10^{9}
Poisson's ratio v	0.3

2.3 Results and Discussion

This section presents and discusses the results obtained for both simply-supported and cantilever blades (beams) subjected to the step load of uniform heat, resulting in time-varying temperature and displacement fields in the blade. Results by the analytical and finite element methods are compared to each other for verification purposes.

2.3.1 Case 1: Simply-supported Beam

Figure 2.8 shows temperature distribution results for the analytical and finite element methods on the top surface ($y=h/2$) of the beam. Results are very close to each other for all the runs. The maximum temperature reaches around 195^{o}C for both methods. The effect of thermal load is then analyzed on thermally-induced vibrations of beams subjected to uniform step heating. Figure 2.9 depicts lateral displacement results for the analytical and 2-D finite element schemes corresponding to $B=\infty$. As seen in the figure, inertia forces disappear and only the static solution remains for the deflection. In Figure 2.10, the lateral displacement of the beam is given for the case when $B=1$. In both Figure 2.9 and Figure 2.10, theoretical and finite element displacement results closely match with each other. The significance of the inertia effects increases as B becomes smaller. If $B=0$, the beam is prevented from deflecting at all at any time.

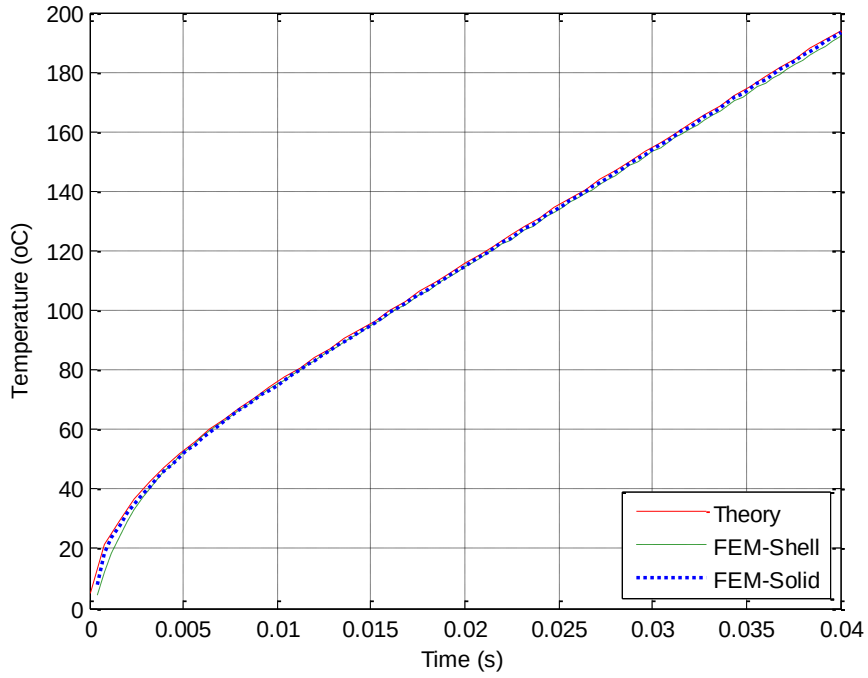

Figure 2.8: Analytical and FEM results for temperature distribution on the top surface of the beam.

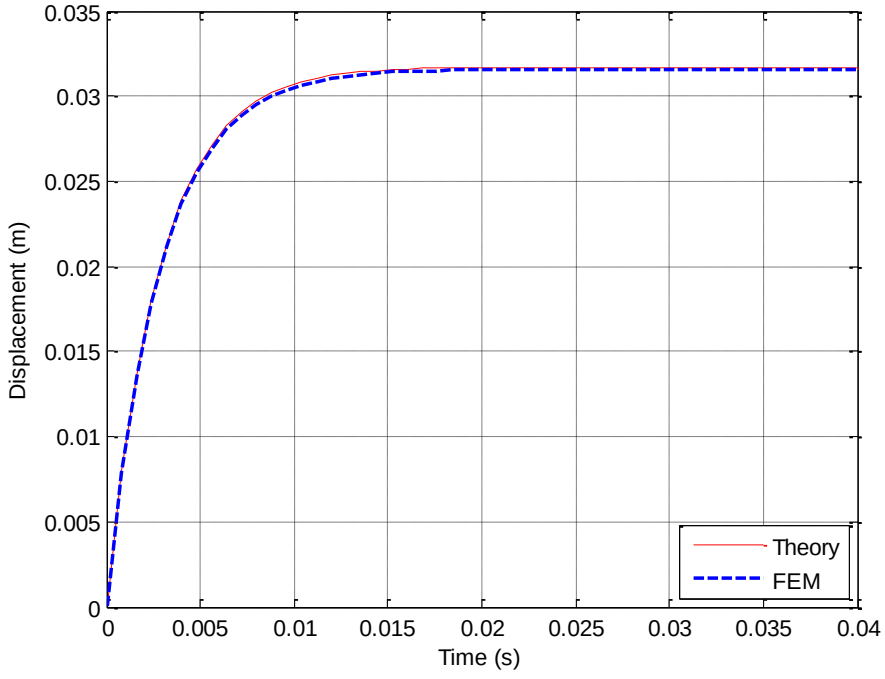

Figure 2.9: Lateral displacement of the uniformly heated simply-supported beam for $B=\infty$.

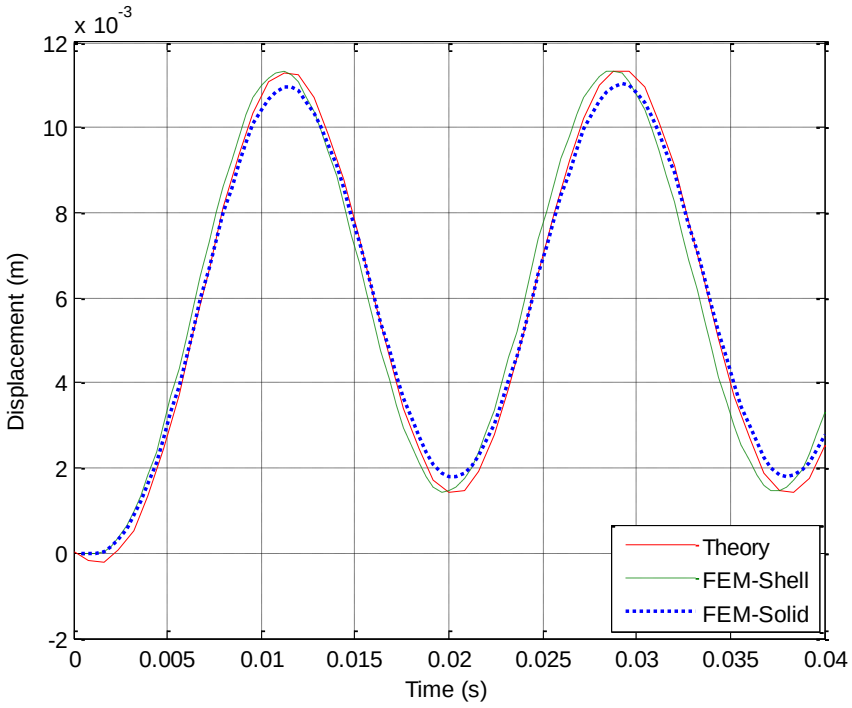

Figure 2.10: Lateral displacement of the uniformly heated simply-supported beam for *B*=1.

2.3.2 Case 2: Cantilever Beam

Temperature distribution of the cantilever beam on its top surface is found analytically and by finite element methods as shown in Figure 2.11. It is very clear that the two results agree with each other very well. Maximum temperature is calculated theoretically as 312.2ºC, which is almost matches the temperature of 310.44 ºC obtained from ANSYS. In Figure 2.12, thermally-induced tip deflection results are shown for only the finite element method due to the absence of the analytical result at this point. But, the fundamental natural frequency for cantilever beam is given from equation (2.21), which is found in this case to be f_n = 55.9 Hz. This value closely matches the approximate fundamental frequency of $\frac{1}{0.0175}$ = 57 Hz in Figure 2.12.

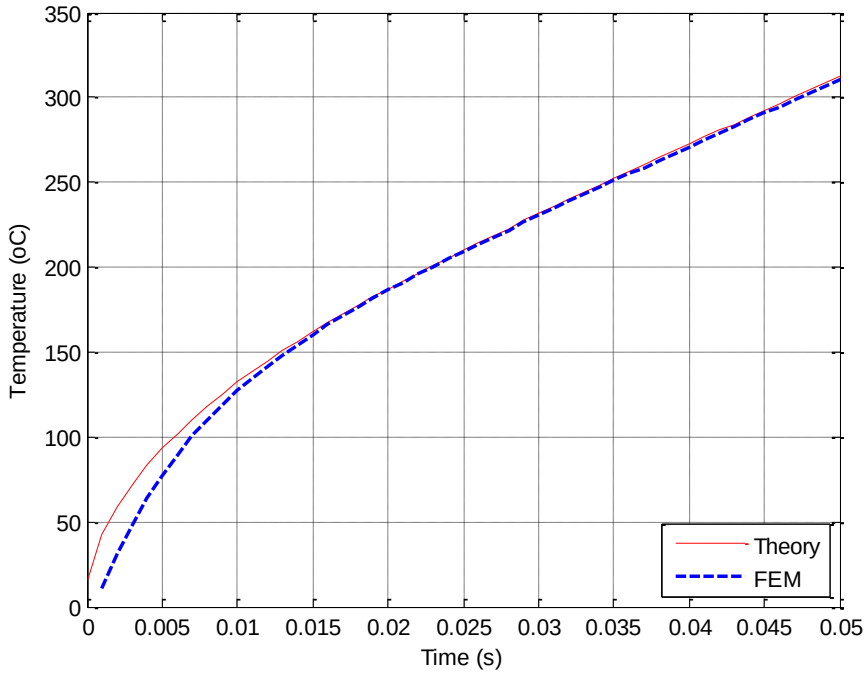

Figure 2.11: Comparison of theory and FEM for temperature distribution of cantilever beam on the top surface.

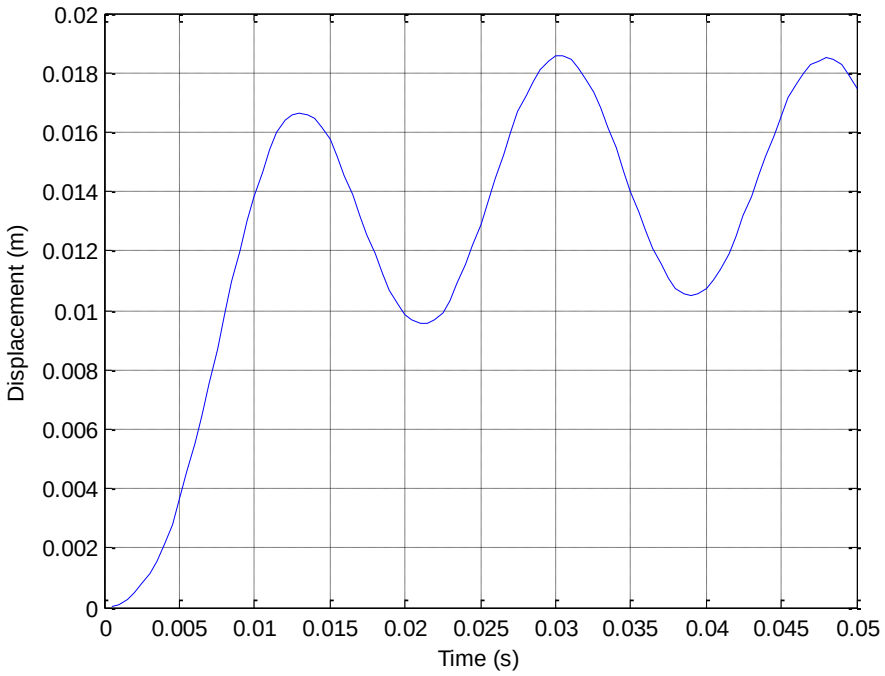

Figure 2.12: Thermally-induced displacement results from ANSYS at the tip of the cantilever beam.

CHAPTER 3

SENSING AND CONTROL OF STATIONARY BLAEDES BY PIEZOECTRIC MATERIALS

In this chapter, sensing and control of stationary cantilever blades (beams/plates) are carried out using the piezoelectric materials bonded at the root of these blades. First, equations of piezoelectricity are presented with material properties of piezoelectricity and the effect of temperature on these properties. Then, piezoelectric sensing and control of stationary blades is carried out and discussed.

3.1 Piezoelectricity

In this research, the Lead Zirconate Titanate (PZT) is used as the piezoelectric material because of its high piezoelectric and dielectric constants. PZT-5A ceramic is utilized for piezoelectric sensing and control because of its high resistivity at elevated temperatures and hence its high curie point of 365^{o}C. A piezoelectric material is modeled in ANSYS using the 3-D coupled-field solid element of SOLID5. Material properties of PZT-5A are given in Table 3.1.

Table 3.1: Material properties of PZT-5A.

c_{11} (Pa)	12.035×10^{10}
c_{12} (Pa)	7.518×10^{10}
c_{13} (Pa)	7.509×10^{10}
c_{23} (Pa)	7.509×10^{10}
c_{22} (Pa)	12.035×10^{10}
c_{33} (Pa)	11.087×10^{10}
c_{44} (Pa)	2.257×10^{10}
c_{55} (Pa)	2.105×10^{10}
c_{66} (Pa)	2.105×10^{10}
e_{31} (C/m^2)	-5.351
e_{33} (C/m^2)	15.783
e_{15} (C/m^2)	12.295
ε_{11} (F/m)	1.5×10^{-8}
ε_{33} (F/m)	1.3×10^{-8}
ρ (kg/m^3)	7800
Curie point (ºC)	365

Finite element equations for piezoelectric materials have already been formulated in many papers. The quadratic form of a thermodynamic potential (energy density) *G* defined as [36]

$$G = \frac{1}{2}S^{\mathrm{T}}cS - \frac{1}{2}E^{\mathrm{T}}\varepsilon E - S^{\mathrm{T}}eE \tag{3.1}$$

The vectors of dielectric and mechanical stress describe the general form of the linear, quasi-static piezoelectric medium equations written as in [37] and [42]:

$$T = \frac{\partial G}{\partial S} = cS - eE \tag{3.2}$$

$$D = -\frac{\partial G}{\partial E} = e^{t}S - \varepsilon E \tag{3.3}$$

For thermopiezoelectricity (piezoelectricity including thermal field), the linear theory assumes a quasi-static motion, which indicates that electrical, thermal, and mechanical forces are equilibrated at any instant. Linear equations of thermopiezoelectricity are written as in [36]:

$$T = c^{E\theta}S - e^{\theta}E - \lambda^{E}\theta \tag{3.4}$$

$$D = \left[e^{\theta}\right]^{t}S + \varepsilon^{S\theta}E + P^{S}\theta \tag{3.5}$$

$$\eta = \{\lambda^{E}\}^{t}S + \{P^{S}\}^{t}E + \alpha\theta \tag{3.6}$$

In the above equations, superscripts denote corresponding constant fields, e.g. $c^{E\theta}$ stands for the elasticity matrix at constant electric field and temperature, etc, while superscript *t* denotes the matrix transpose.

where:

T: Vectors of mechanical stress.

D: Vectors of charge per unit area (electric displacement).

S: Vectors of mechanical strain.

E: Vectors of electric field.

λ: Coefficients of thermal stress

P: Coefficients of pyroelectricity.

d: The matrix of coefficients of direct piezoelectric effect.

e: The matrix of piezoelectric coefficients

ε: The matrix of dielectric

c: The matrix of elastic.

η: Scalar of entropy density, and

α: Scalar of thermal constitutive coefficient.

The energy functional equation Π, is expressed in order to obtain the dynamic piezoelectric equations:

$$\Pi = \int_V G dV - \int_V u^{\mathrm{T}} P_b dV - \int_S u^{\mathrm{T}} P_s dV - u^{\mathrm{T}} P_c + \int_S \emptyset \sigma dS \qquad (3.7)$$

where P_b, P_s, P_c, $\emptyset$, and σ denote vectors of body, surface, concentrated forces, electrical potential, and surface charge, all in respective order.

The dynamic coupled equations of piezoelectric medium are solved using the finite element method together with Hamilton's principle defined as in [38]:

$$\delta \int_{t_1}^{t_2} (Ki - \Pi) dt = 0 \tag{3.8}$$

where *Ki*, the kinetic energy, can be written as:

$$Ki = \int_V \frac{1}{2} \rho \dot{u}^{\mathrm{T}} \dot{u} dt \tag{3.9}$$

where ρ and $\dot{u}$ standing for the mass density and the velocity vector, respectively. Now equation 3.8 can be re-written by using equation 3.9 as:

$$\delta \int_{t_1}^{t_2} \Pi dt = \delta \int_{t_1}^{t_2} Ki \, dt = - \int_{t_1}^{t_2} \int_V \rho \delta u^{\mathrm{T}} \ddot{u} dV dt \tag{3.10}$$

The virtual change in the potential *G* found using integration by parts of equation 3.10 with proper boundary conditions as shown

$$\delta G = \delta S^{\mathrm{T}} T - \delta E^{\mathrm{T}} D \tag{3.11}$$

The finite element modeling approximations, for the mechanical displacement and electrical potential in general form, are written as

$$u_{el} = N_u u_i \tag{3.12}$$

$$\emptyset_{el} = N_{\emptyset}\emptyset_i \tag{3.13}$$

where u_{el}, ϕ_{el}, u_i, ϕ_i, N_u, and N_φ stand for the displacement vector, the electrical potential pertaining to the finite element, the nodal displacement, and electrical potential vectors, and the shape function matrices for both the displacement and electrical fields, all in respective order. Subscripts *el* and *i* indicate the finite element and nodes of the element.

The following relations for mechanical strain and electrical field in the piezoelectric medium are expressed as in [37]:

$$S_{el} = L_u u_{el} = [L_u N_u]u_i = B_u u_i \tag{3.14}$$

$$E_{el} = -\nabla\emptyset_{el} = -[\nabla N_{\emptyset}]\emptyset_i = -B_{\emptyset}\emptyset_i \tag{3.15}$$

Where L_u and ∇ stand for differential operator matrix and gradient vector, which are expressed as

$$L_u = \begin{bmatrix} \frac{\partial}{\partial x} & 0 \\ 0 & \frac{\partial}{\partial y} \\ \frac{\partial}{\partial y} & \frac{\partial}{\partial x} \end{bmatrix} \tag{3.16}$$

$$\nabla = \begin{bmatrix} \frac{\partial}{\partial x} \\ \frac{\partial}{\partial y} \end{bmatrix} \tag{3.17}$$

The dynamic coupled ordinary differential equations of piezoelectric medium was found by substituting finite element approximations represented in equations 3.12 and 3.13 in

equations 3.14 and 3.15, then substituting these in turn in equations 3.7 and 3.9 in the generalized Hamilton's principle given in equation 3.8. This yields the following:

$$M_{uu}\ddot{u} + K_{uu}u + K_{u\emptyset}\emptyset = F \tag{3.18}$$

$$K_{\emptyset u}u - K_{\emptyset\emptyset}\emptyset = G_c \tag{3.19}$$

The finite element matrices and vectors in equations 3.18 and 3.19 are computed as follows

$$\begin{gathered}
[M_{uu}]_{el} = \int_{V_{el}} \rho_{el} N_u^{\mathrm{T}} N_u dV,\ [K_{uu}]_{el} = \int_{V_{el}} B_u^{\mathrm{T}} c_{el} B_u dV \\
[K_{u\emptyset}]_{el} = [K_{u\emptyset}]_{el}{}^{\mathrm{T}} = \int_{V_{el}} B_u^{\mathrm{T}} e_{el} B_\emptyset dV \\
F_{el} = \int_{V_{el}} N_u^{\mathrm{T}} P_{b\,el} dV + \int_{S_e} N_u^{\mathrm{T}} P_{s\,el} dS + N_u^{\mathrm{T}} P_{c\,el} \\
G_{c\,el} = -\int_{S_{el}} N_\emptyset^{\mathrm{T}} \sigma_{el} dS
\end{gathered} \tag{3.20}$$

Where G_c is the applied charge vectors, this discusses in the following sections as PZT actuator input V_a for the purpose of control.

From the ANSI (IEEE) standards given in [39], the constitutive matrices for piezoelectric materials are as in the following three matrices:

1. The piezoelectric relative permittivity (dielectric property matrix with constant strain) matrix:

$$\varepsilon^S = \begin{bmatrix} \varepsilon_{11} & 0 & 0 \\ 0 & \varepsilon_{11} & 0 \\ 0 & 0 & \varepsilon_{33} \end{bmatrix} \mathrm{F/m} \tag{3.6}$$

2. The piezoelectric elastic property matrix with constant electric field (stiffness matrix):

$$C^E = \begin{bmatrix} C_{11} & C_{12} & C_{13} & 0 & 0 & 0 \\ C_{12} & C_{11} & C_{13} & 0 & 0 & 0 \\ C_{13} & C_{13} & C_{33} & 0 & 0 & 0 \\ 0 & 0 & 0 & C_{44} & 0 & 0 \\ 0 & 0 & 0 & 0 & C_{44} & 0 \\ 0 & 0 & 0 & 0 & 0 & C_{66} \end{bmatrix} \mathrm{N\ m^{-2}} \tag{3.7}$$

3. The piezoelectric strain coefficient matrix:

$$e = \begin{bmatrix} 0 & 0 & e_{31} \\ 0 & 0 & e_{31} \\ 0 & 0 & e_{33} \\ 0 & e_{15} & 0 \\ e_{15} & 0 & 0 \\ 0 & 0 & 0 \end{bmatrix} \mathrm{C\ m^{-2}} \tag{3.8}$$

3.1.1 Effect of Temperature on Piezoelectric Properties

Temperature can affect the material properties of piezoelectric sensors made of PZT-5A such as thermal expansion coefficient and dielectric permittivity. If this effect is neglected, data obtained from piezoelectric sensors may not accurately represent the actual behavior of the structure.

Thermal Expansion Coefficient

The thermal expansion coefficient α of PZT-5A will change as the temperature increases from 0 ºC to 200 ºC as shown below in Table 3.2 [40].

Table 3.2: Thermal expansion coefficient α of PZT-5A in 1/K.

Temperature ºC	0	50	100	150	200
α_x	1×10^{-6}	1.4×10^{-6}	2×10^{-6}	2.7×10^{-6}	3.3×10^{-6}
α_y	1×10^{-6}	1.4×10^{-6}	2×10^{-6}	2.7×10^{-6}	3.3×10^{-6}
α_z	4×10^{-6}	4×10^{-6}	3×10^{-6}	1×10^{-6}	1.6×10^{-6}

Dielectric Permittivity

The dielectric permittivity in constant strain (ε^S) of PZT-5A changes roughly in a linear fashion with temperature. Raising the temperature from 0 ºC to 200 ºC increases the dielectric permittivity by almost 50% as seen below in Table 3.3 [41].

Table 3.3: Dielectric permittivity ε^S of PZT-5A in (F/m).

Temperature ºC	0	50	100	150	200
ε_x	8.11×10^{-9}	9.86×10^{-9}	11.6×10^{-9}	11.9×10^{-9}	12.2×10^{-9}
ε_y	8.11×10^{-9}	9.86×10^{-9}	11.6×10^{-9}	11.9×10^{-9}	12.2×10^{-9}
ε_z	7.35×10^{-9}	8.26×10^{-9}	9.175×10^{-9}	10.09×10^{-9}	11×10^{-9}

3.2 Piezoelectric Sensing of Stationary Blades

The cantilever beam considered in Chapter 2, is now mounted with piezoelectric patches of PZT-5A on its bottom and top surfaces at its root as shown in Figure 3.1. Just as in Section 2.2.2, the length, width and thickness (height) of the steel beam are taken as L=0.122 m, b=0.02525 m, and h=0.001 m. As for the two PZT layers, the length, width and thickness are assumed to be L=0.012625 m, b=0.02525 m, and h=0.001 m. Material properties for the steel beam and PZT-5A are listed before in Table 2.2 and Table 3.1, respectively.

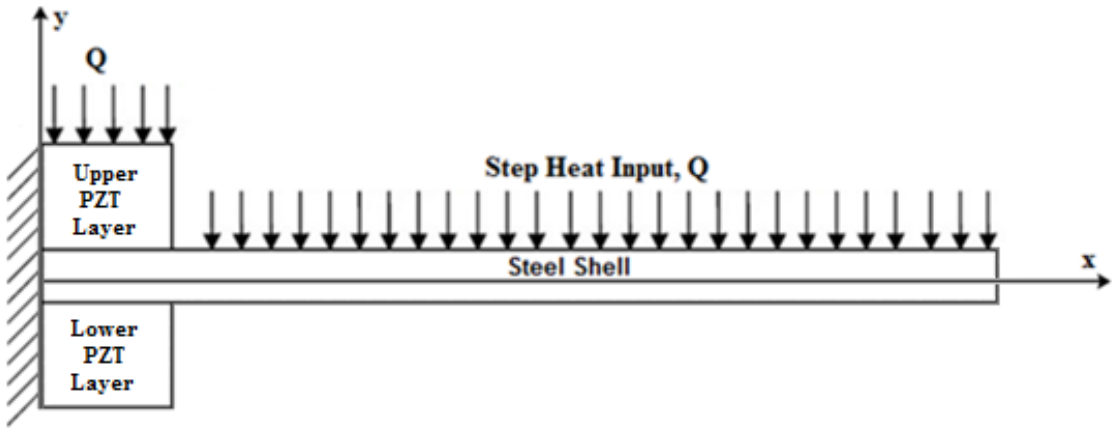

Figure 3.1: Cantilever plate with piezoelectric (PZT) layers (not to scale).

The system of cantilever plate with upper and lower PZT layers is tested for temperature distribution and lateral displacement in cantilever plate, and voltage in lower PZT layer. As shown in Figure 3.1, the system of the cantilever blade together with the upper and the lower PZT layers is fixed at its end edge for translations and rotations.

A step heat input of $Q = 1\times10^6$ W/m^2 is applied on the top surface of the plate and PZT layer, while the convection heat transfer of the system is taken to be h = 10 W/m^{2}K on the remaining surfaces. The PZT layers are grounded at the boundary with the blade

for reference. A proportional damping of $2\zeta\omega_n = 2\zeta(2\pi f_n) = 4\pi\zeta f_n = 4\pi(0.01)\ 67.31 = 8.5$ is assumed for thermally-induced vibrations.

The cantilever plate (blade) and the PZT layers are simulated each in ANSYS using the 3-D coupled field solid elements. The blade is modeled using the element "SOLID226" where thermal and structural fields are both coupled, while the PZT layers are modeled using element type "SOLID5" that couples thermal, structural, and electrical fields, respectively. The finite element mesh of the system consisting of the steel plate and two PZT-5A layers with the thermal input can be seen in Figure 3.2 and Figure 3.3. The finite element mesh of the system has resulted in 600 finite elements and 4,297 nodes in total.

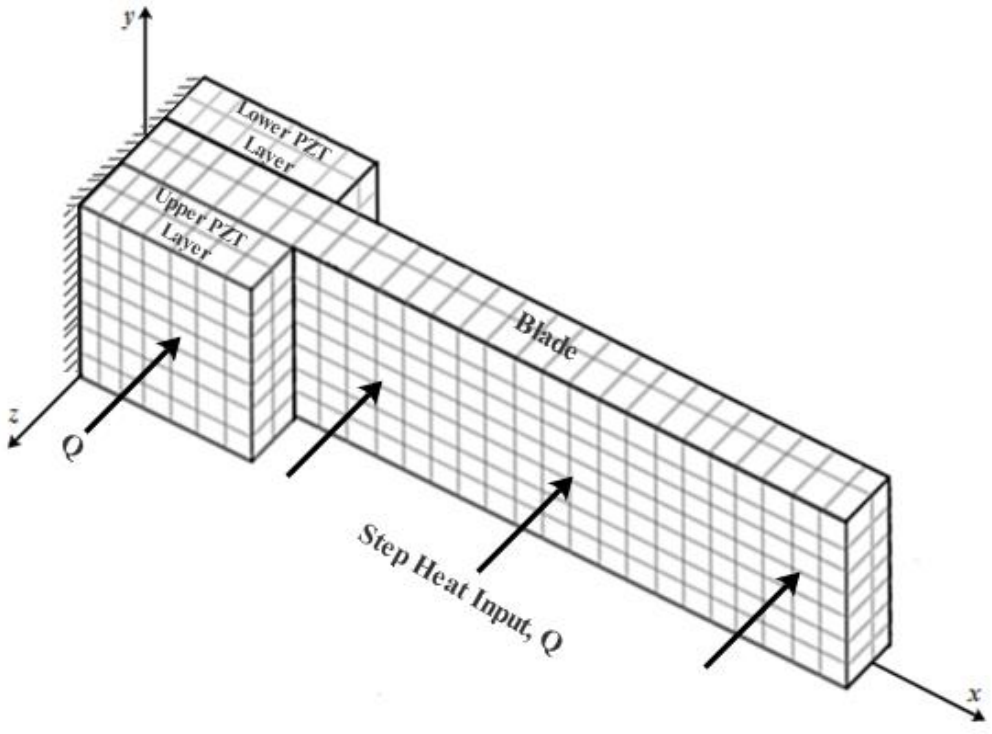

Figure 3.2: Finite element mesh of the system with thermal load (not to scale).

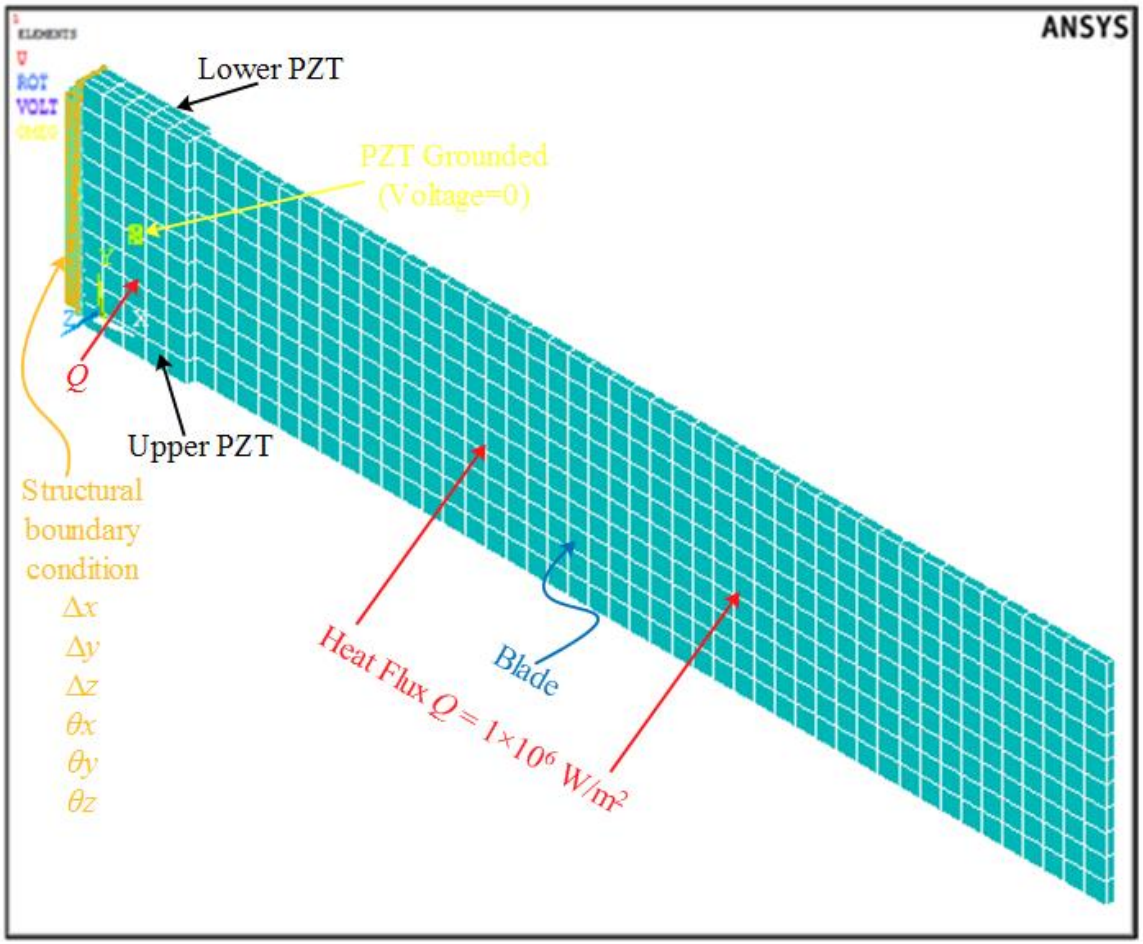

Figure 3.3: Finite element model in ANSYS.

The temperature is found for both the plate and PZT layers using the analytical (theoretical) method in section 2.1.1 and the finite element method via ANSYS. Figure 3.4 shows that the temperatures of the plate are very close to each other for both the analytical and the finite element methods. This figure indicates that temperature of the plate reaches a maximum value of 47.13ºC, which is virtually equal to the temperature found theoretically as 47ºC. However, Figure 3.5 shows that the nodal temperature of the upper PZT layer climbs to a high value of 193.4ºC at its top-right corner.

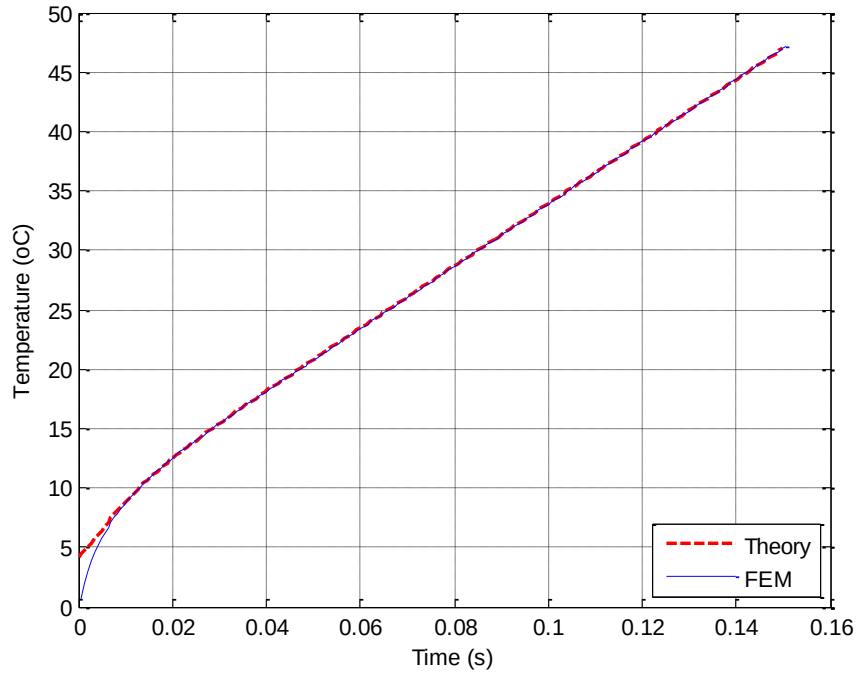

Figure 3.4: Nodal temperature of the plate.

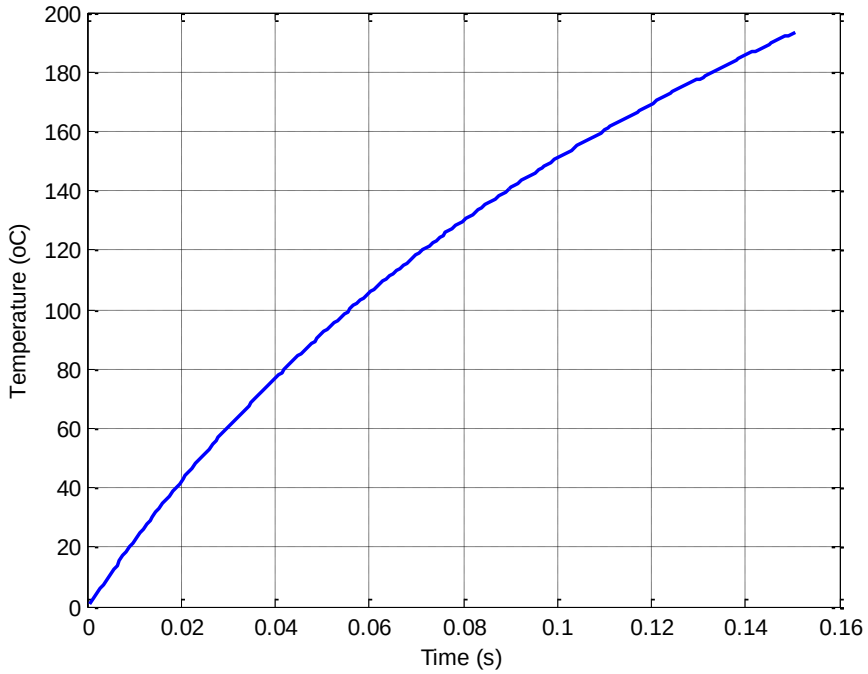

Figure 3.5: Nodal temperature of the upper PZT layer at the top-right corner.

The thermally-induced vibration of the system subjected to the above temperature distribution is now studied for the lateral displacement in the plate and voltage in the PZT layers. Both the plate displacement and PZT voltage outputs are also used for the modal analysis to determine natural frequencies of the system. Figure 3.6 and Figure 3.7 show displacement and voltage responses of the system, whereas Figure 3.8 depicts the FFT results of both responses. Figure 3.8 clearly shows that the fundamental lowest natural frequency of the system from both the displacement and voltage outputs is 67.31 Hz.

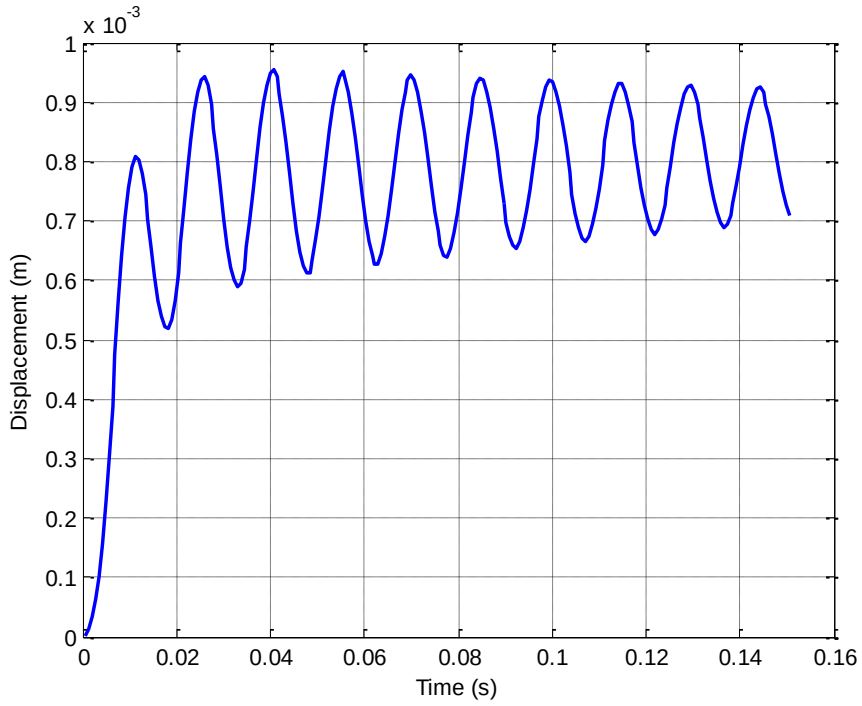

Figure 3.6: Tip deflection of the cantilever plate.

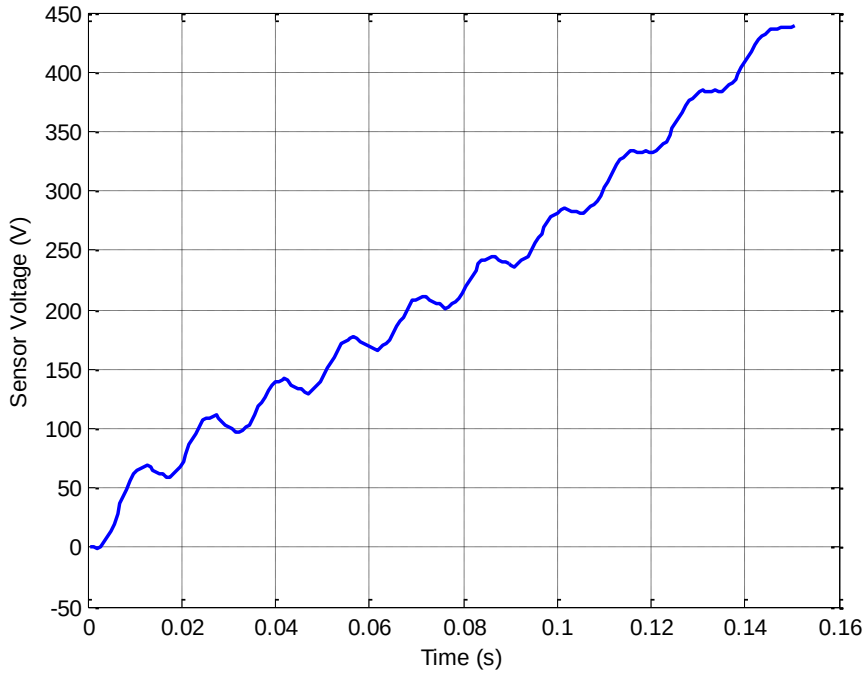

Figure 3.7: Voltage output at the corner of the PZT layer.

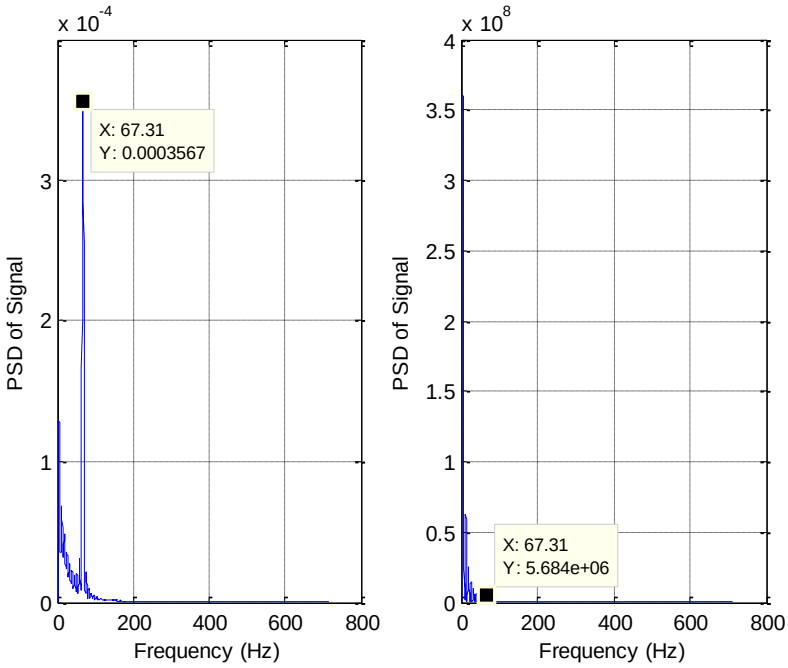

Figure 3.8: Power Spectral Density (PSD) of the plate's deflection (left) and PZT's voltage (Right).

3.3 Piezoelectric Control of Stationary Blades

The closed-loop diagram of the 'smart structure' is shown in Figure 3.9. Without loss of generality, tip deflection of the cantilever blade, herein called u_y, is fed back to the feedback control scheme, which multiplies velocity v_y of the signal by a negative gain of g_v and sends it to the summer to compare it against the reference voltage of R found from the static analysis. Hence, the feedback voltage V_a fed to the piezoelectric actuator (bottom PZT layer in Figure 3.2 and Figure 3.3) is given as

$$V_a = R + g_v v_y \tag{3.9}$$

The feedback voltage V_a is applied to the PZT actuator on its whole bottom surface. As mentioned previously, surfaces of both the PZT layers glued on the blade are grounded.

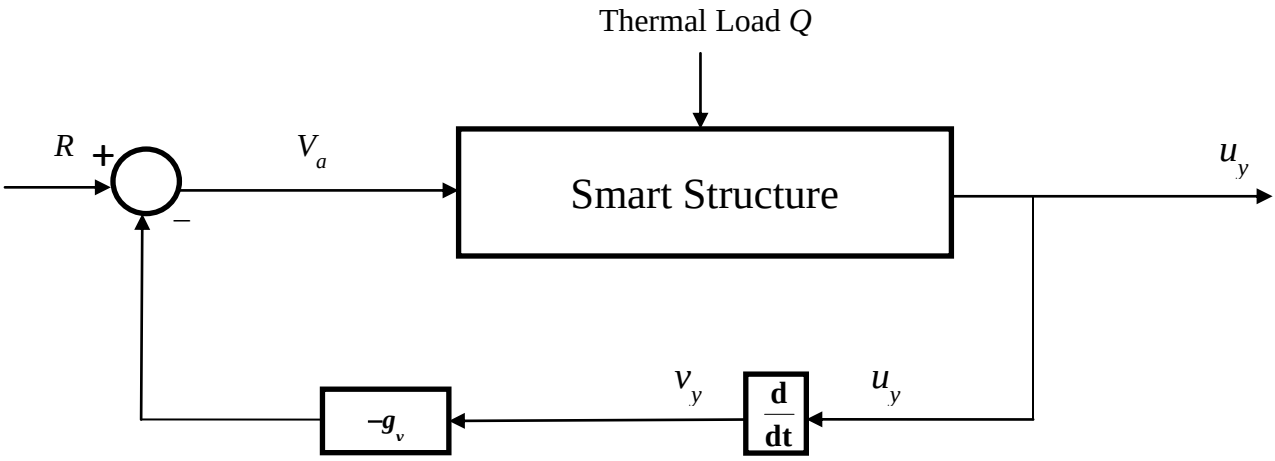

Figure 3.9: Piezoelectric control system for the stationary smart blade.

Temperature distribution on the top surface of the plate shown in Figure 3.10 shows no difference in open and closed-loop behaviors due to its non-oscillating nature. Responses of the closed-loop stationary smart system are shown in Figures 3.11 through 3.13. Figure 3.11 depicts the open and closed-loop (control off and on) tip deflections of

the cantilever plate. As seen clearly in this figure, the piezoelectric feedback control scheme forces the vibration of the system to converge to its steady-state in a short period of time of about 0.1 sec. As stated in Section 3.2, a proportional damping of 8.5 is assumed for thermally-induced vibrations. Figure 3.12 and Figure 3.13, illustrate sensor and actuator voltages when the controller is on and off. Vibrations are fast attenuated in voltages of both the lower sensor and upper actuator layers.

Furthermore, figures 3.15 to 3.17 show tip deflection of the cantilever blade, PZT sensor and actuator voltages for different values of the feedback gain g_v in respective order. When g_v is zero, there is no control action and hence the actuator voltage is zero (Figure 3.17) and the system oscillates with its existing proportional damping (Figure 3.15 and Figure 3.16). It is clear in these figures that the system converges to its steady-state faster with increasing g_v. Moreover, increasing temperature causes the sensor voltage to climb as the time goes on. It is also due to differences in material properties, especially in thermal expansion coefficients that resulting thermal stress differences between the two materials (steel for the blade and PZT for the piezoelectric layers) make them behave in different ways to thermally-induced vibrations.

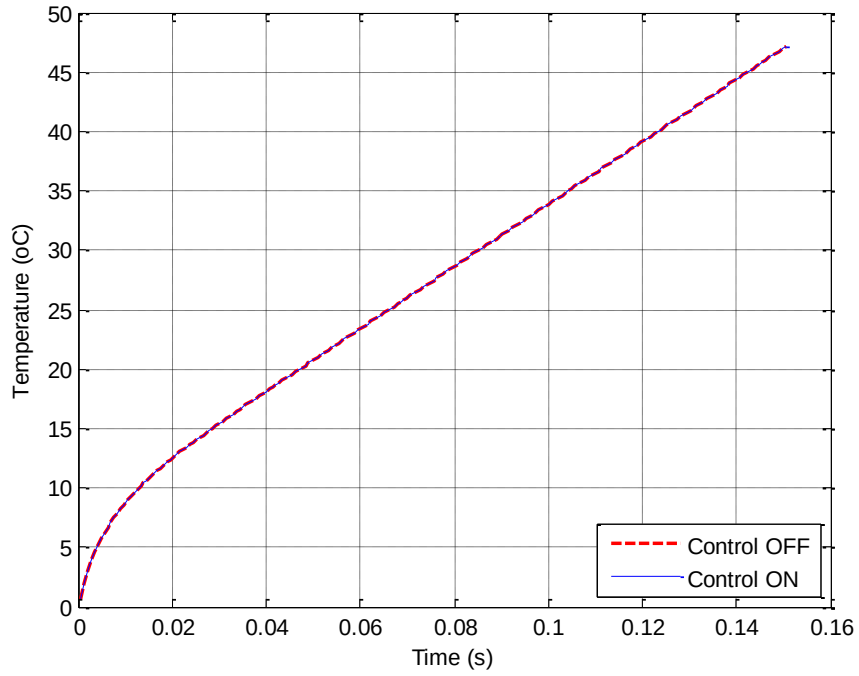

Figure 3.10: Temperature increase on top surface of the cantilever blade.

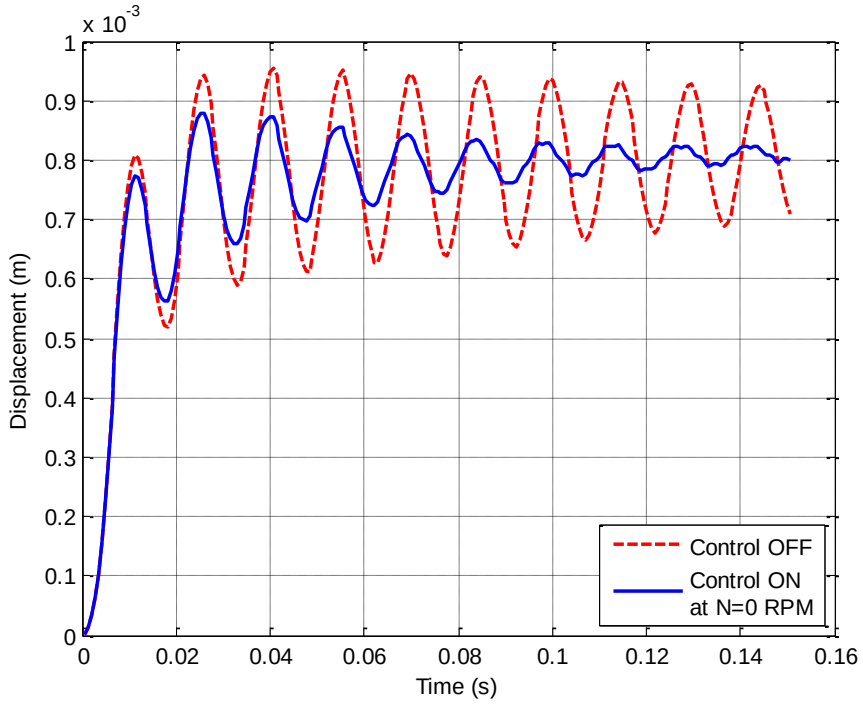

Figure 3.11: Tip deflection of the cantilever blade.

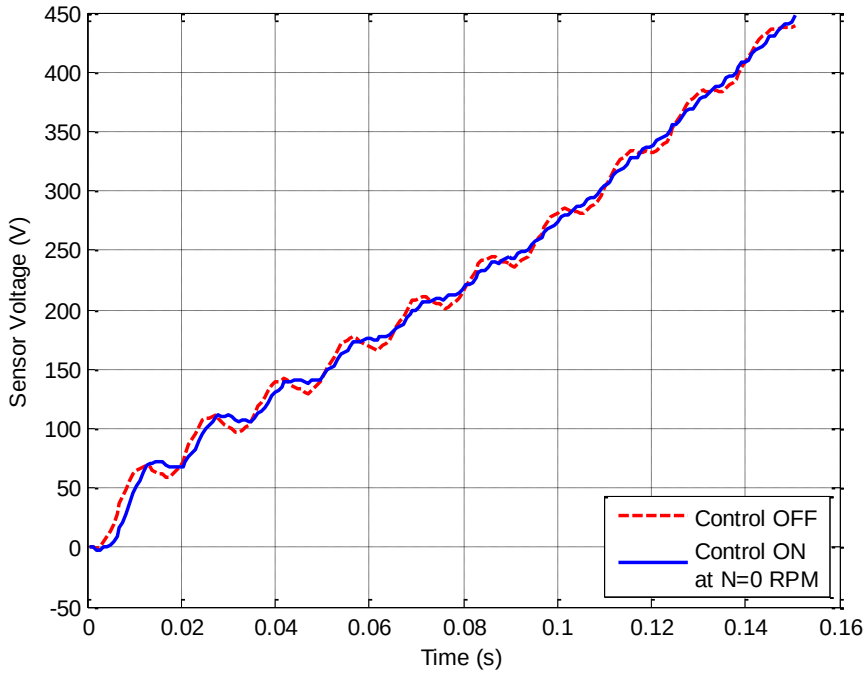

Figure 3.12: PZT sensor voltage of the cantilever blade.

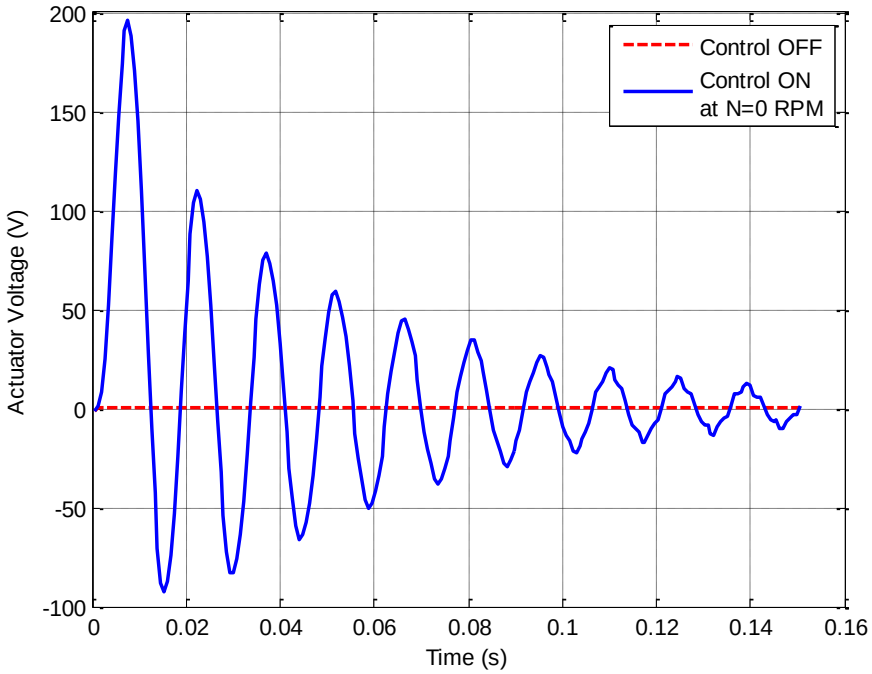

Figure 3.13: PZT actuator voltage of the cantilever blade.

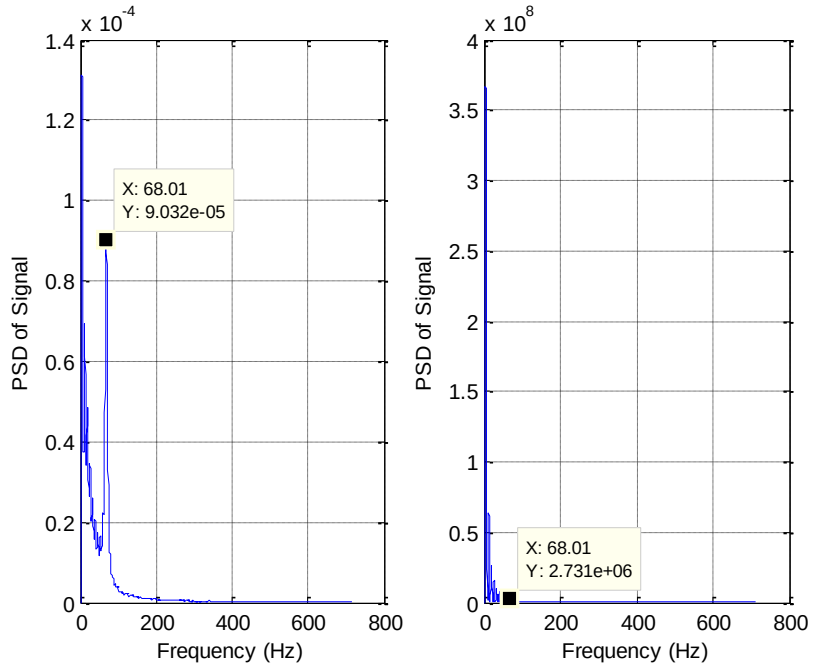

Figure 3.14: Power Spectral Density (PSD) of the plate's deflection (left) and PZT's voltage (Right).

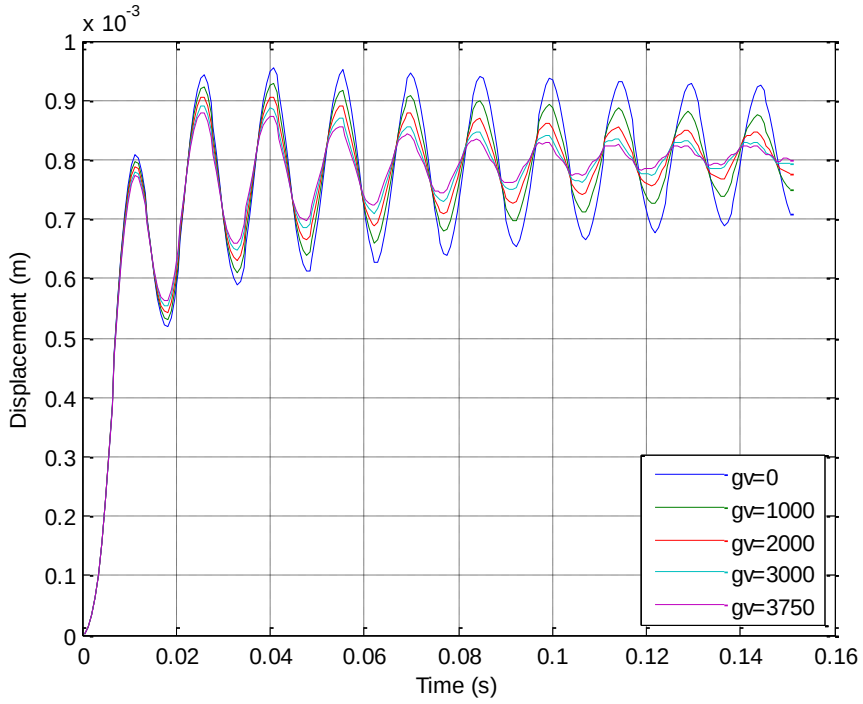

Figure 3.15: Tip deflection of the cantilever blade with different feedback gains of g_v.

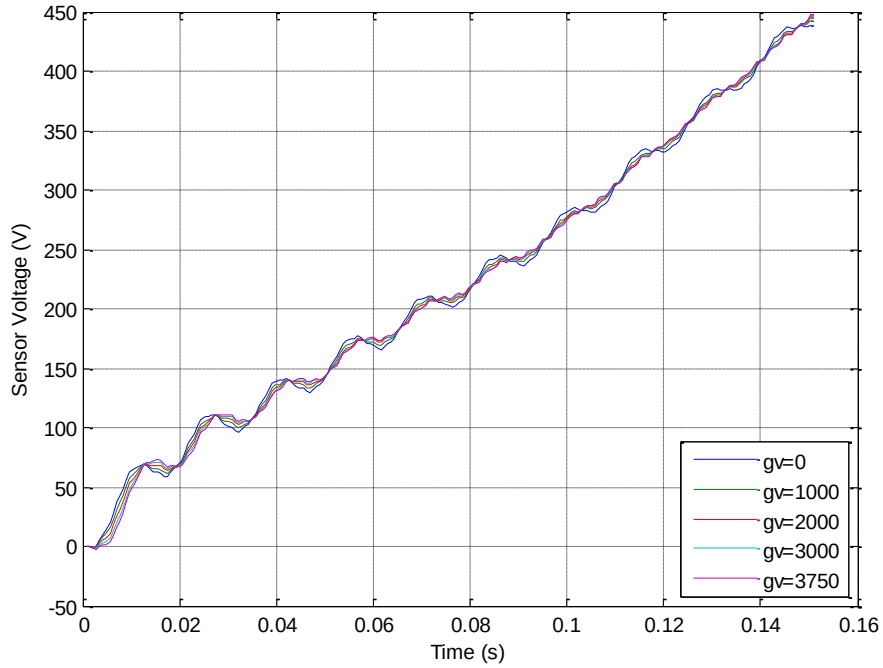

Figure 3.16: PZT sensor voltages of the cantilever blade with different feedback gains of g_v.

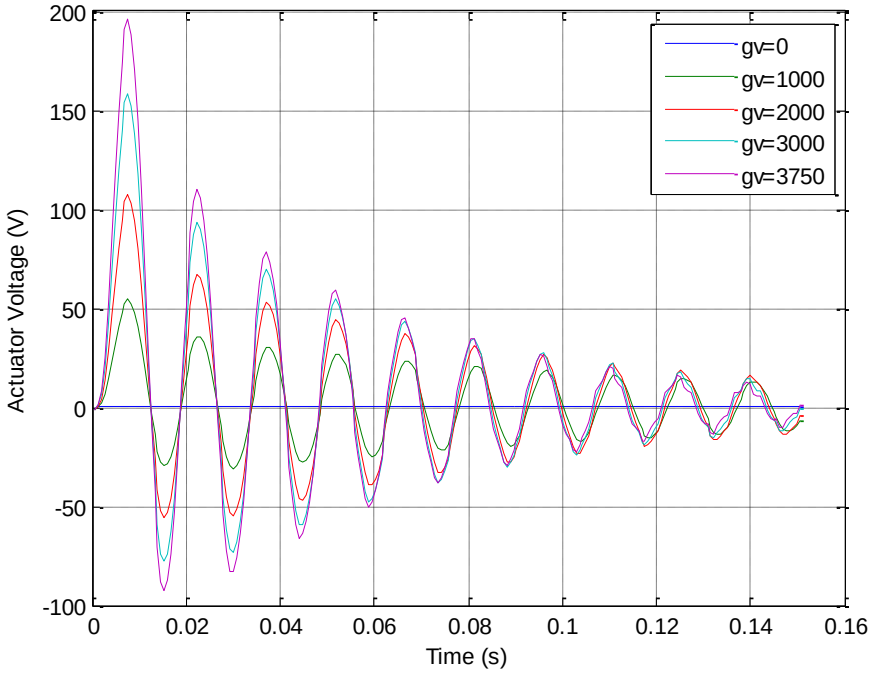

Figure 3.17: PZT actuator voltages of the cantilever blade with different feedback gains of g_v.

Damping ratios (ζ) and maximum sensor and actuator voltages (V_{smax} and V_{amax}) of the stationary blade with different values of feedback gain are given in Table 3.4, which indicates that as the feedback gains increase, control actions increase, whereas maximum sensor voltages are kept below the limit of 500 V.

Table 3.4: Damping ratio (ζ), maximum sensor and actuator voltages (V_{smax} and V_{amax}) of stationary blade.

Rotational Speed (RPM)	0				
g_v	0	1000	2000	3000	3750
ζ	0.0041	0.0146	0.0244	0.0361	0.0495
V_{smax} (V)	439.229	443.327	445.558	446.979	447.832
V_{amax} (V)	0. 001085	54.3882	107.283	158.725	196.376

CHAPTER 4

THERMALLY-INDUCED VIBERATION SENSING AND CONTROL FOR ROTATING BLADES

The rotating blade problem is solved for temperature distribution in this chapter in response to the thermal load as defined in Chapter 3. The calculated temperature distribution is then imposed on the blade to obtain its lateral displacements. The piezoelectric sensing is first considered and is followed by the control action.

4.1 Piezoelectric Sensing of Rotating Blades

The stationary blade studied in Chapter 3 is now given three different rotational speeds, which are: N=1,200, 2,400 and 3,600 rev/min (RPM), or ω=125.66, 251.3 and 377 rad/s. The temperature distribution followed by thermally-induced lateral displacement and PZT voltage results are shown in Figures 4.1 through 4.9. Fundamental natural frequencies are evident in FFT plots of the plates tip displacement and PZT's voltage in Figure 4.3, Figure 4.6 and, Figure 4.9, which clearly indicate natural frequencies of 68.71, 71.5 and 75.68 Hz at the corresponding speeds of 1,200, 2,400 and 3,600 RPM, respectively. Hence, fundamental natural frequencies assume higher values with increases in rotational speeds. This is due to the combined effects of stress-stiffening and spin-softening for rotating blades. The fundamental natural frequencies in PZT sensor voltages' responses in Figure 4.3, Figure 4.6 and, Figure 4.9 are dominated by the

static response and hence they are not easily distinguishable in FFT plots. However, the time plots of the PZT sensor voltages clearly indicate the existence of these natural frequencies.

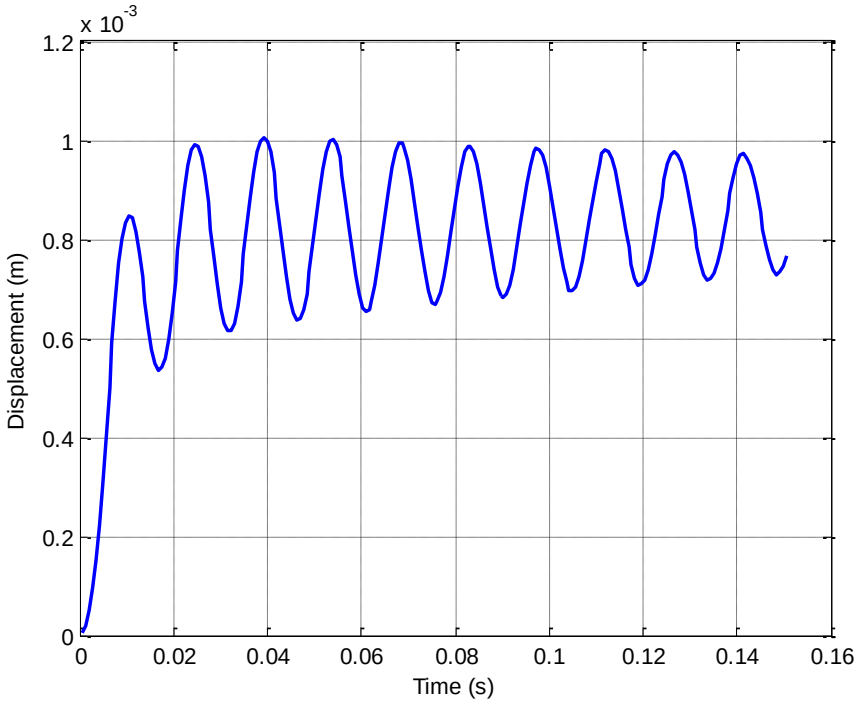

Figure 4.1: Tip deflection of the plate at N=1,200 RPM.

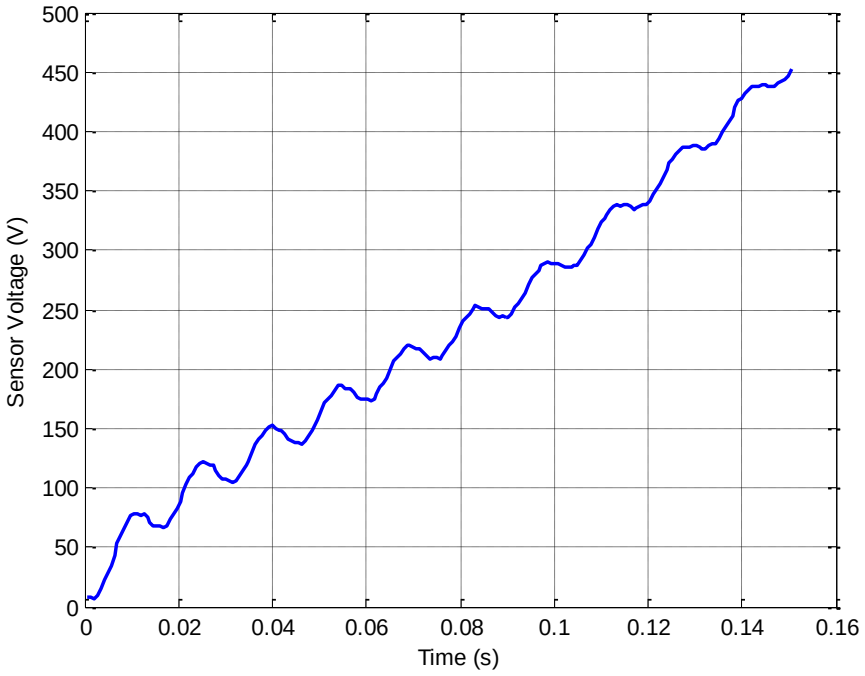

Figure 4.2: Voltage at the tip of the piezoelectric layer at *N*=1,200 RPM.

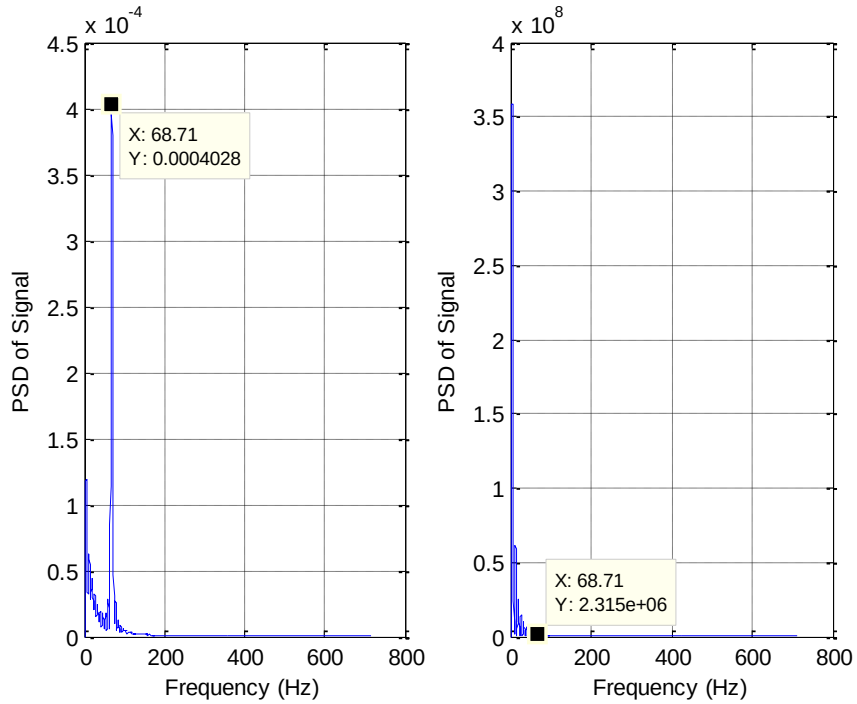

Figure 4.3: FFT of plate's displacement (left) and PZT's voltage (right) at *N*=1,200 RPM.

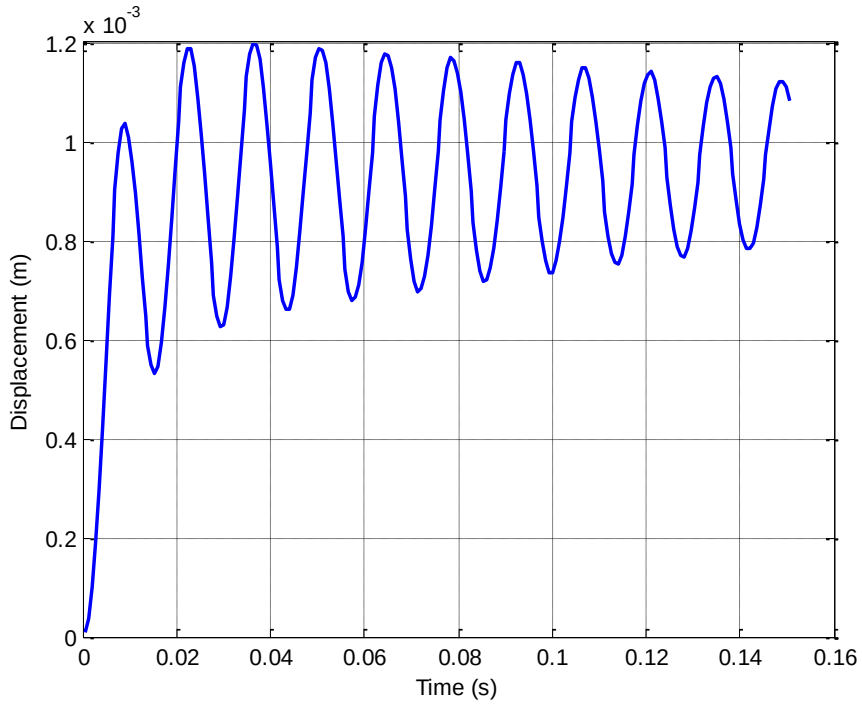

Figure 4.4: Tip deflection of the plate at *N*=2,400 RPM.

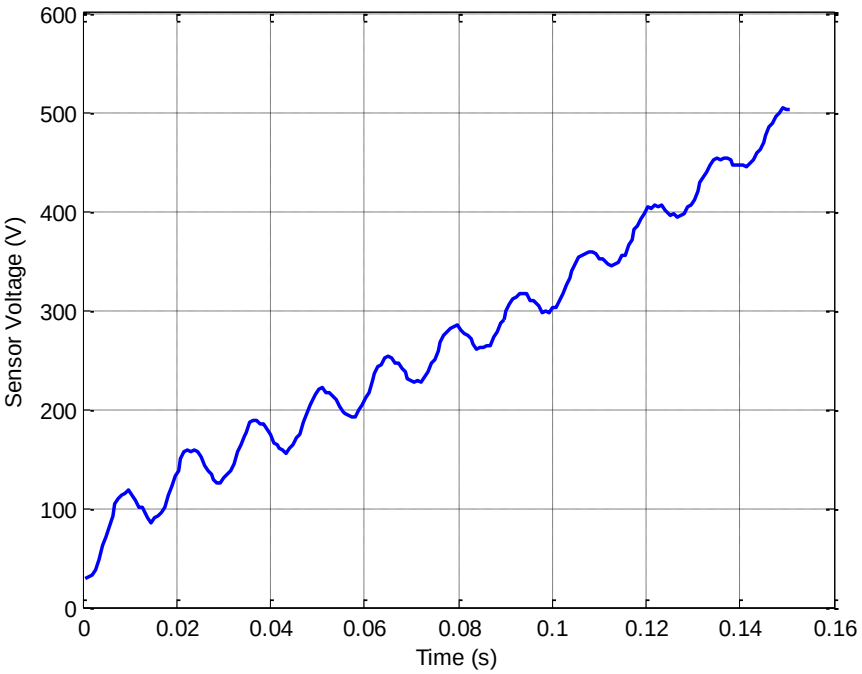

Figure 4.5: Voltage at the tip of the piezoelectric layer at *N*=2,400 RPM.

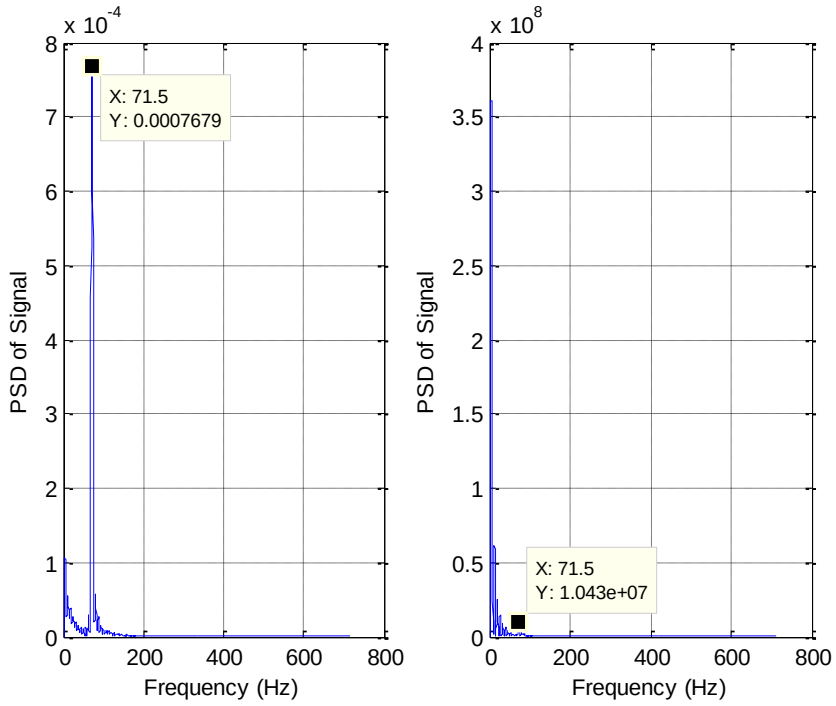

Figure 4.6: FFT of plate's displacement (left) and PZT's voltage (right) at *N*=2,400 RPM.

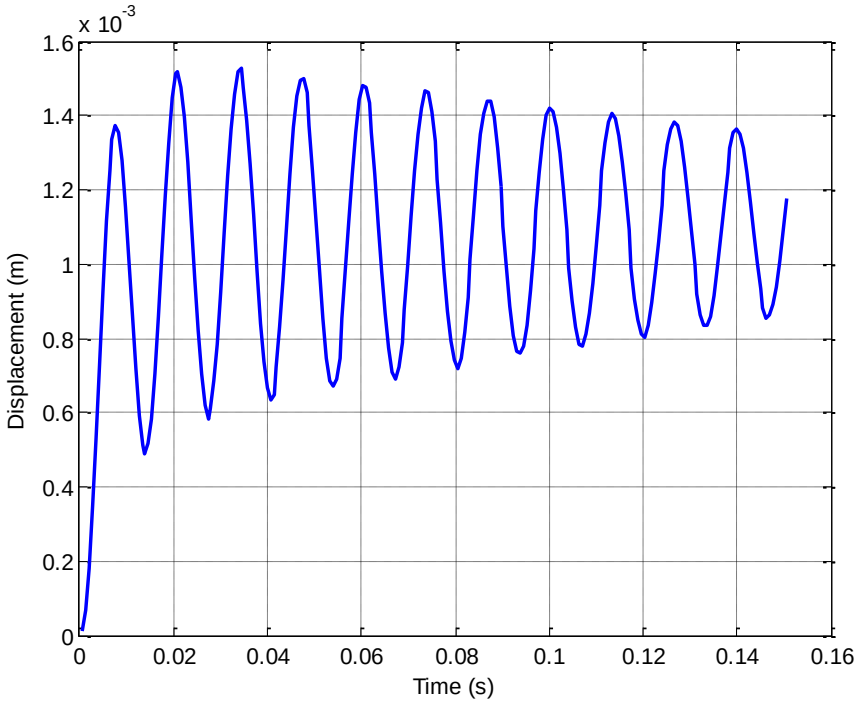

Figure 4.7: Tip deflection of the plate at *N*=3,600 RPM.

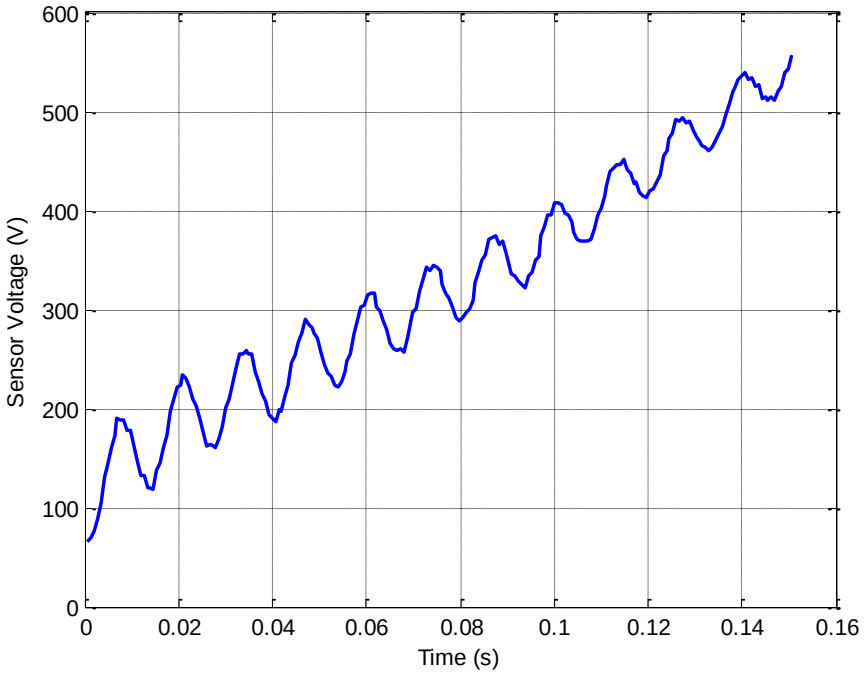

Figure 4.8: Voltage at the tip of the piezoelectric layer at *N*=3,600 RPM.

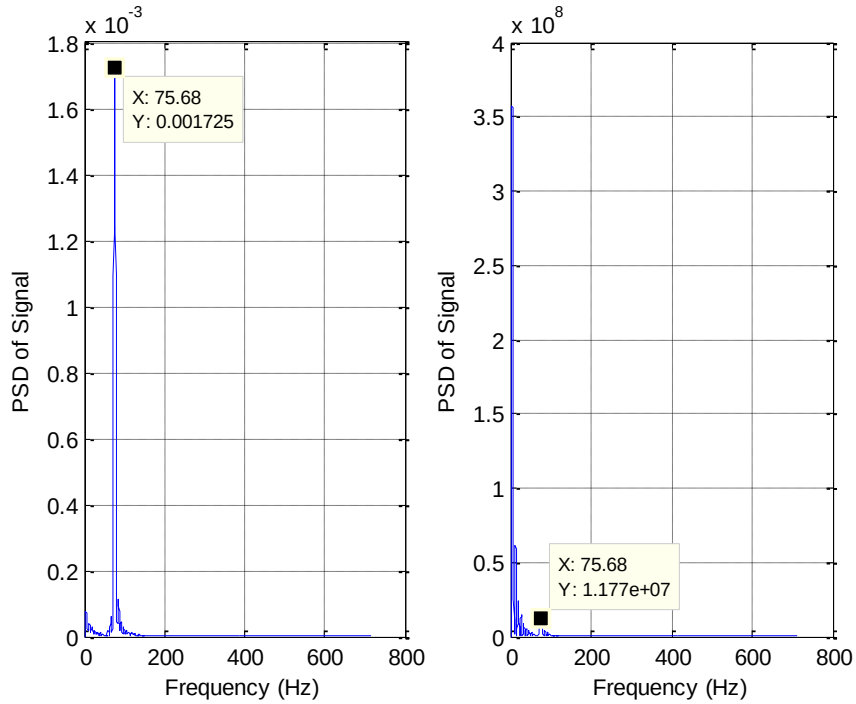

Figure 4.9: FFT of plate's displacement (left) and PZT's voltage (right) at *N*=3,600 RPM.

4.2 Piezoelectric Control of Rotating Blades

Responses for the cantilever plate at rotational speeds of 1200, 2400 and 3600 RPM with the control actions are solved for the blade displacement, sensor and actuator voltages.

Results for both open and closed-loop responses shown in Figures 4.11 through 4.22 for the noted rotational speeds indicate good performance of control actions because of less overshoot and settling time in closed-loop behavior. In all these results, the value of the negative feedback g_v is taken as 3,750 for the maximum control performance. Figure 4.10 shows the temperature increase plot at the top-right corner of the upper PZT layer (sensor) onto which the thermal load of $Q = 1\text{x}10^6$ W/m^2 is applied. Neither the control action nor the rotation rate makes any difference for the temperature distribution, which reaches a maximum value of 193.4^{o}C at the end of the control period. This maximum temperature is much less than the Curie point of PZT-5A that is noted as 365^{o}C in Table 3.1.

Figure 4.11, Figure 4.15, and Figure 4.19 depict the vertical tip displacement of the blade at the middle node. As shown clearly in these figures, the response of the open-loop system decays to approach the steady-state after a certain time because of the proportional damping of the system. However, the closed-loop response decays asymptotically into the steady state in order to settle down faster. The sensor voltages are shown in Figure 4.12, Figure 4.16 and Figure 4.20, which illustrate oscillations with increasing static voltage values due to differences in material properties between the blade and piezoelectric layers. Figure 4.13, Figure 4.17 and Figure 4.21 show actuator

voltages with and without control actions at different speeds, which indicate fast convergence to zero after the control is over. Figure 4.14, Figure 4.18 and Figure 4.22 give results for the FFT plots showing increasing trends of fundamental natural frequencies as the speeds increase due to spin-softening and stress-stiffening effects. These natural frequencies are easy to distinguish in tip deflection plots, but not in sensor voltages, due to dominance of static voltages as the time progresses.

Table 4.1 lists changes in fundamental natural frequencies of f_n at the above-mentioned speeds with and without control actions. This table indicates small increases in these frequencies for the closed-loop system due to slight modification of system matrices resulting from the feedback control scheme. The following tables, Tables 4.2 through 4.4, list results for the damping ratios (ζ) which is calculated from equation 2.24, maximum sensor and actuator voltages (V_{smax} and V_{amax}) at different speeds of N and feedback gains of g_v. It is important to note in these tables that the maximum sensor and actuator voltages are kept within the limits of 500 V per mm of the PZT layer thickness. The voltage and temperature limits are crucial for the piezoelectric materials to retain their properties in order to function as sensors and actuators. As expected, damping ratios and maximum actuator voltages given in Tables 4.2 to 4.4 indicate increasing values as the feedback gains increase, and hence control actions increase, whereas maximum sensor voltages are kept below the limit of around 500 V in all cases. If found excessive, the amount of this maximum voltage could be reduced to a smaller value by tuning the feedback gain to a lower level.

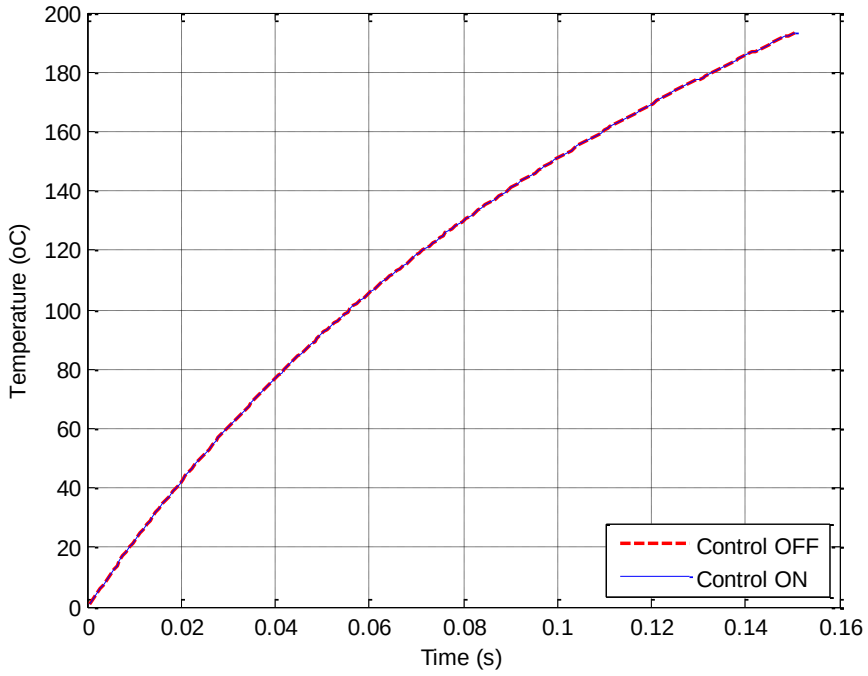

Figure 4.10: Temperature increase of the upper PZT layer (sensor) at the top-right corner.

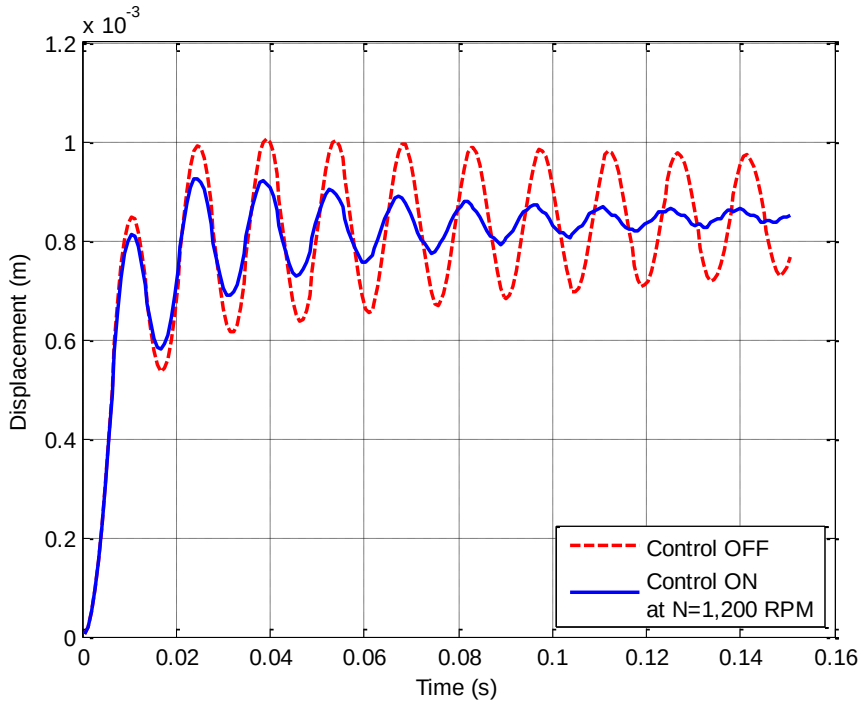

Figure 4.11: Tip deflection of the cantilever blade at *N*=1,200 RPM.

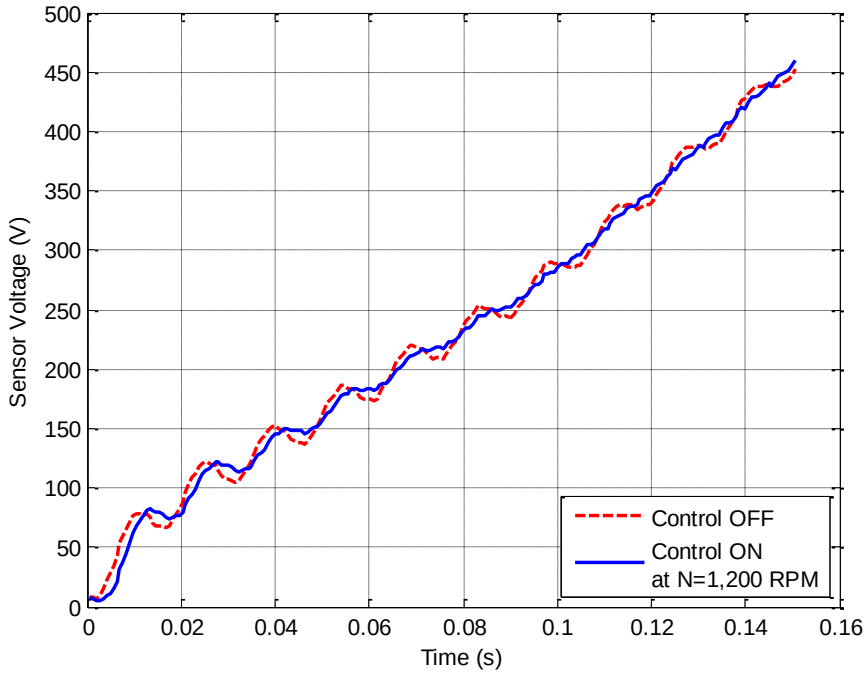

Figure 4.12: PZT sensor voltage of the cantilever blade at *N*=1,200 RPM.

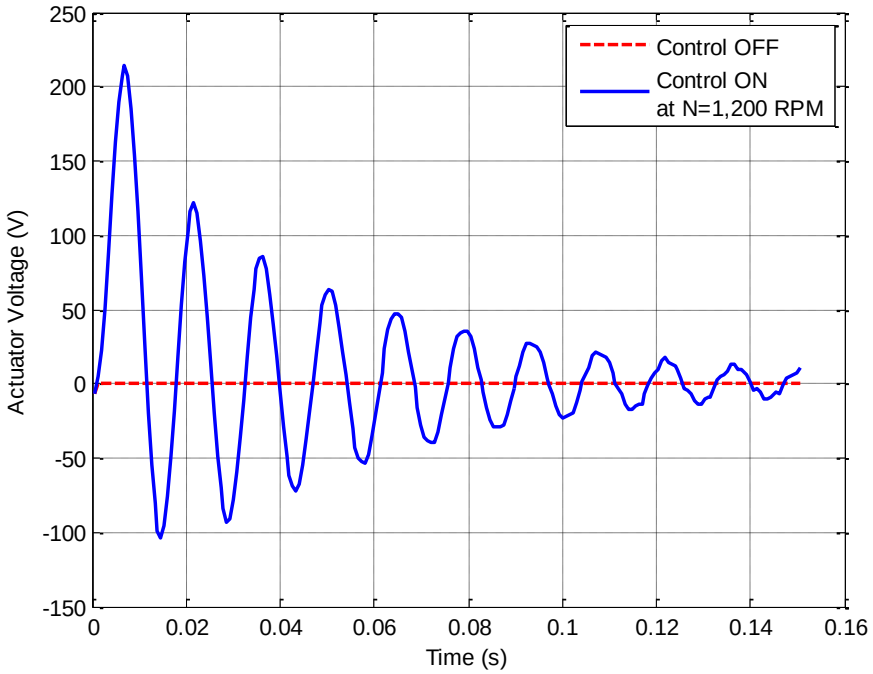

Figure 4.13: PZT actuator voltage of the cantilever blade at *N*=1,200 RPM.

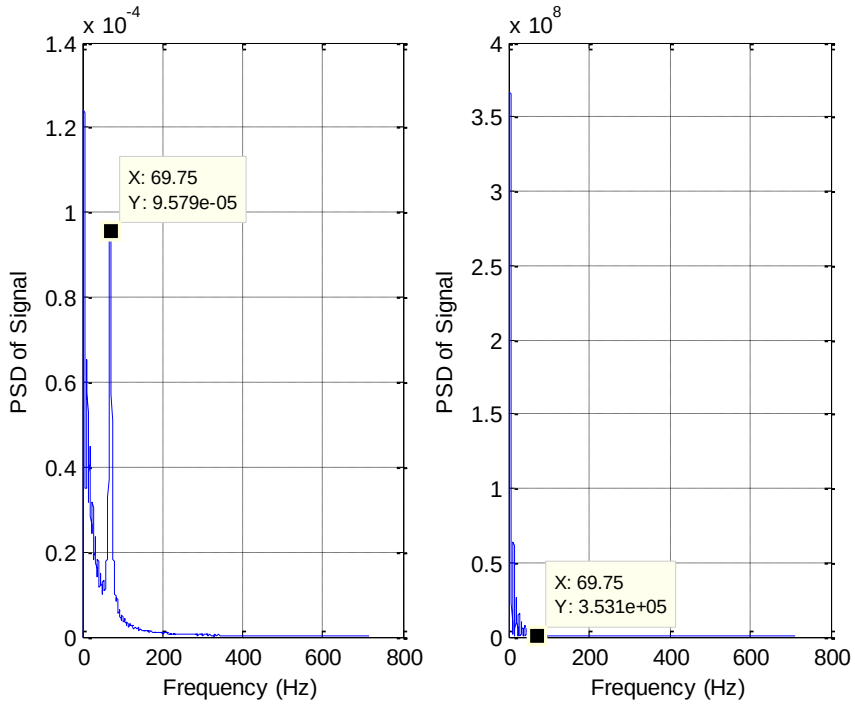

Figure 4.14: FFT of plate's displacement (left) and PZT's voltage (right) at *N*=1,200 RPM.

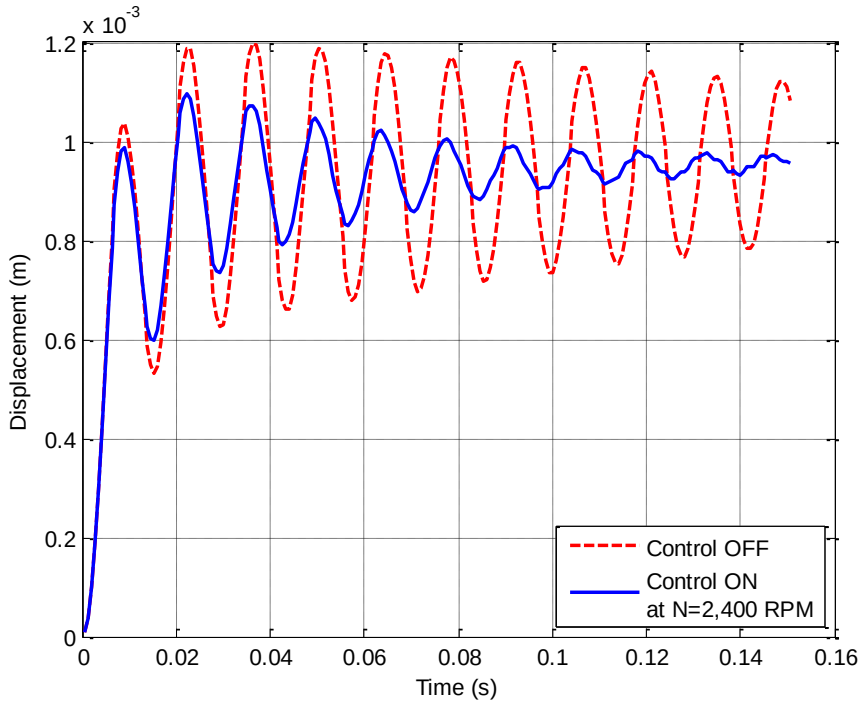

Figure 4.15: Tip deflection of the cantilever blade at *N*=2,400 RPM.

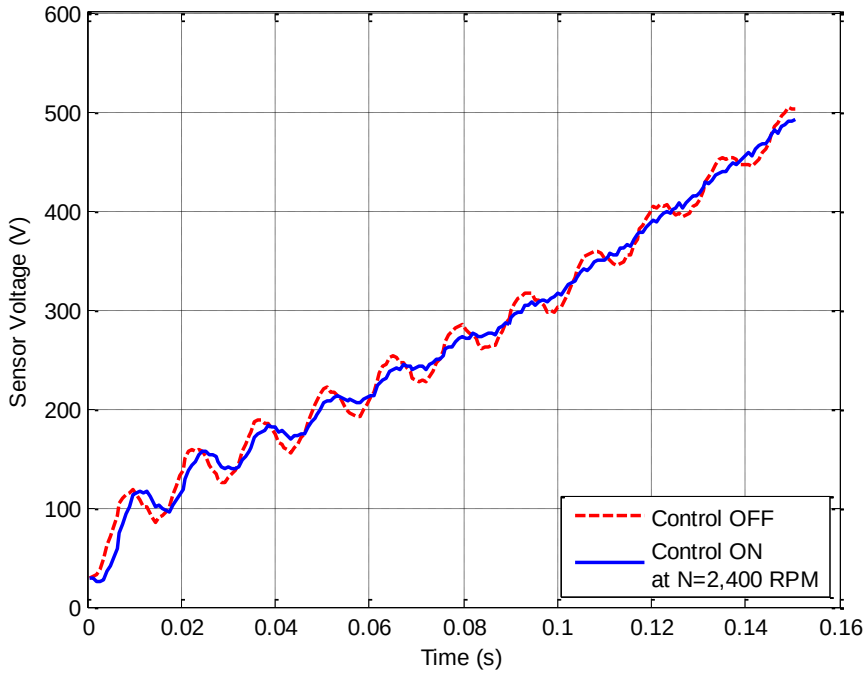

Figure 4.16: PZT sensor voltage of the cantilever blade at *N*=2,400 RPM.

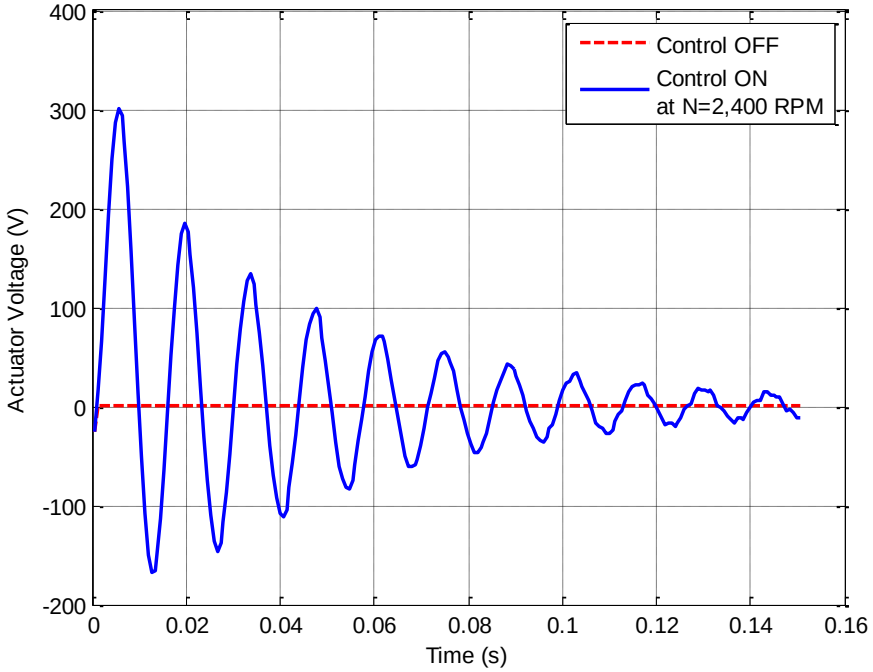

Figure 4.17: PZT actuator voltage of the cantilever blade at *N*=2,400 RPM.

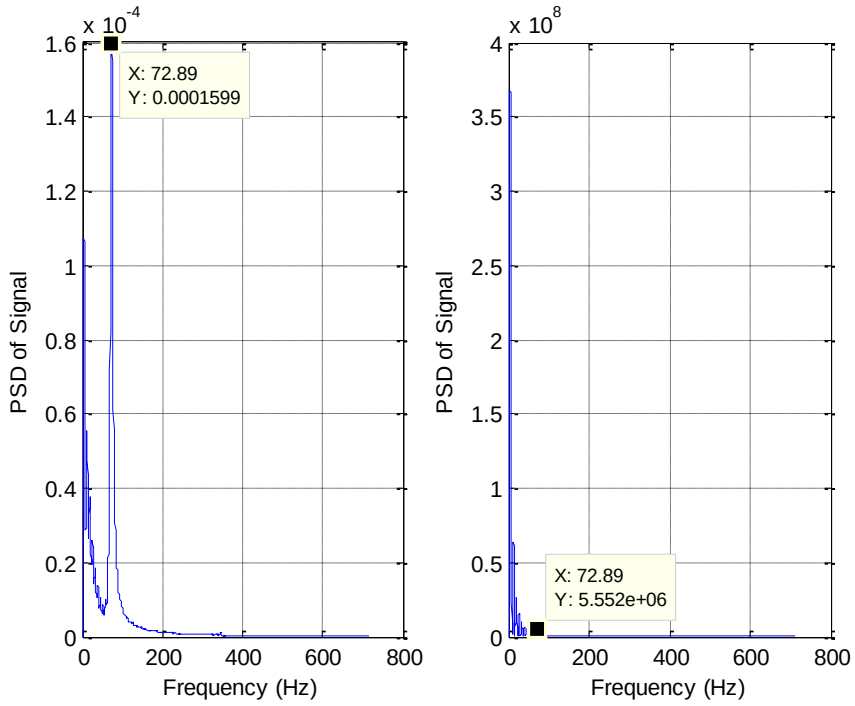

Figure 4.18: FFT of plate's displacement (left) and PZT's voltage (right) at *N*=2,400 RPM.

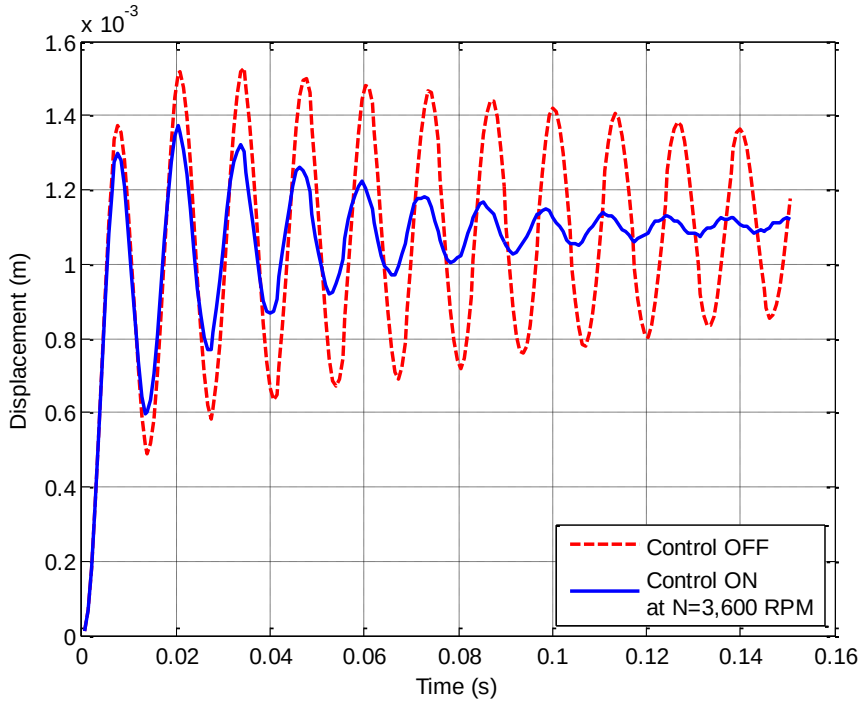

Figure 4.19: Tip deflection of the cantilever blade at *N*=3,600 RPM.

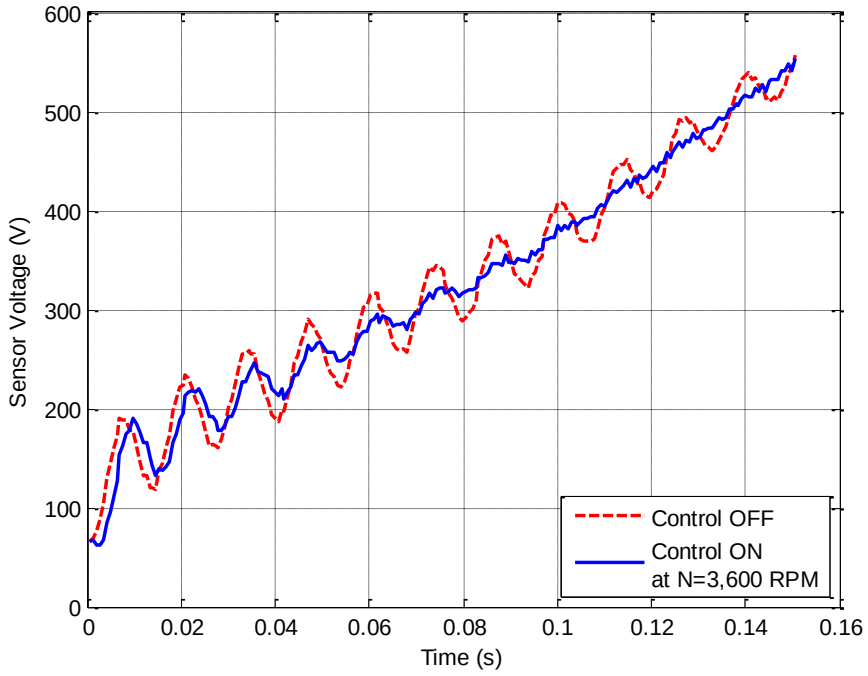

Figure 4.20: PZT sensor voltage of the cantilever blade at *N*=3,600 RPM.

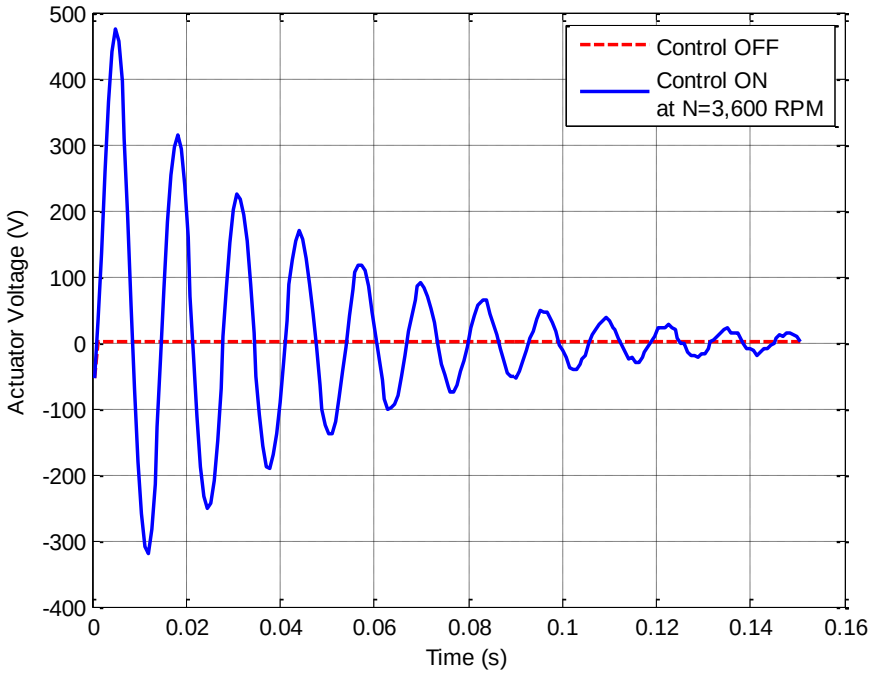

Figure 4.21: PZT actuator voltage of the cantilever blade at *N*=3,600 RPM.

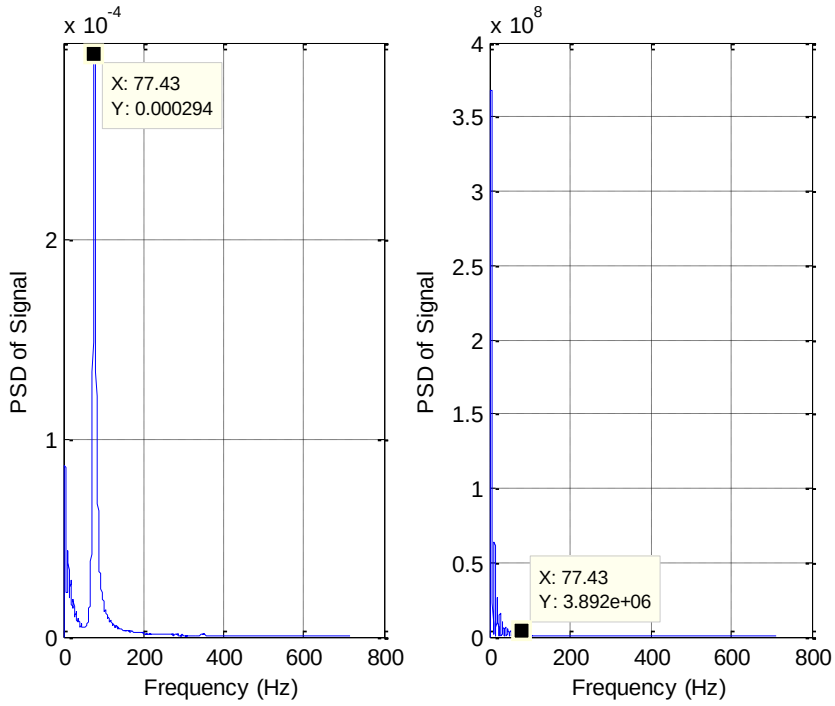

Figure 4.22: FFT of plate's displacement (left) and PZT's voltage (right) at N=3,600 RPM.

Table 4.1: Natural frequencies of the blade before and after control actions.

Rotational Speed (RPM)	Natural frequencies (Hz)	
	f_n before control	f_n after control
0	67.31	68.01
1,200	68.71	69.75
2,400	71.5	72.89
3,600	75.68	77.43

Table 4.2: Damping ratio (ζ), maximum sensor and actuator voltages (V_{smax} and V_{amax}) at N=1,200 RPM.

g_v	0	1000	2000	3000	3750
ζ	0.0054	0.017	0.0246	0.0368	0.0498
V_{smax} (V)	453.091	456.661	458.436	459.489	460.053
V_{amax} (V)	0.001085	59.4144	117.192	173.377	214.495

Table 4.3: Damping ratio (ζ), maximum sensor and actuator voltages (V_{smax} and V_{amax}) at N=2,400 RPM.

g_v	0	1000	2000	3000	3750
ζ	0.0067	0.0174	0.0281	0.0406	0.0550
V_{smax} (V)	502.727	496.877	494.274	492.955	492.361
V_{amax} (V)	0. 001085	83.0918	164.154	243.229	301.257

Table 4.4: Damping ratio (ζ), maximum sensor and actuator voltages (V_{smax} and V_{amax}) at N=3,600 RPM.

g_v	0	1000	2000	3000	3750
ζ	0.101	0.0195	0.0322	0.0468	0.0579
V_{smax} (V)	557.250	555.522	554.208	553.752	553.682
V_{amax} (V)	0.001085	130.326	257.709	382.203	473.71

CHAPTER 5

CONCLUSIONS AND FUTURE WORK

5.1 Conclusions

Thermally-induced vibration sensing and control of blades are considered in this thesis work. Temperature distribution is first analyzed for a simply-supported beam along its thickness due to a uniform heat flux, followed by the lateral vibrations of the beam caused by the temperature gradients over the thickness. This well-known problem is solved analytically for the purpose of verifying of the finite element method through the ANSYS program. Both the temperature distribution and lateral vibrations of the beam agree with each other well using the analytical and finite element approaches.

A cantilever blade problem is considered next for the thermally-induced vibrations, because blades of turbo-machinery are best modeled as cantilevered beams, plates and/or shells. The cantilever beam problem is again checked against the analytical method for its temperature distribution solution obtained by the finite element method. The two methods have resulted in almost identical solutions. Finite element results of thermally-induced vibrations of the blade are also verified by the analytical solutions available in the literature for the first fundamental natural frequency of the cantilever blade.

The cantilever blade is then mounted with a PZT-5A piezoelectric sensor and actuator at its fixed root for sensing and actuation. Constant heat flux is applied from the

upper surfaces of both the PZT sensor and the blade, while the other surfaces are assumed to have natural heat convection to their surroundings. Resulting voltages are confined to a maximum voltage of 500 V per mm of the PZT layer thickness and temperatures to values much less than the Curie point of 365^{o}C for proper functioning of piezoelectric elements. The output voltage of the upper PZT sensor obtained without any control action is found to be oscillating with increasing static values and fundamental natural frequency of the system. The increasing nature of the output voltage is attributed to differences in thermal material properties of the blade and piezoelectric layers. These differences yield thermal stresses between the two materials, which in return cause the PZT sensor output voltage to climb.

The control action is performed by feeding the tip deflection of the blade to the PZT actuator after taking its time derivative and then multiplying it by a constant negative feedback gain. Both stationary and rotating blades are considered for sensing and control. Increasing the amplitude of the feedback gain leads to faster control action with less overshoot and settling time, as expected. Damping ratios and maximum actuator voltages also increase, but maximum sensor voltages stay around the limit of 500 V.

With or without the control of the system, the fundamental natural frequency of the system increases as the rotational speed increases due to effects known as spin-softening and stress-stiffening. The control action applied in this work pushes the closed-loop natural frequency slightly higher compared with the open-loop due to changes in closed-loop system matrices.

5.2 Future Work

The study in this thesis could be followed up by the works listed below:

a) Other control schemes, in addition to the velocity feedback with constant negative gain considered in this work, can be looked into for possibly improved closed-loop behavior.

b) A system of bigger scale can be taken as rotating machinery with rotating blades and their control can be investigated for thermally-induced vibrations.

c) Various other heat inputs such as impulse or sinusoidal types can be studied both analytically and numerically using the finite element method.

d) Whenever possible and feasible, experimental set-ups would also be useful to further verify the results.

APPENDIX

I. PROGRAMING FLOW CHART

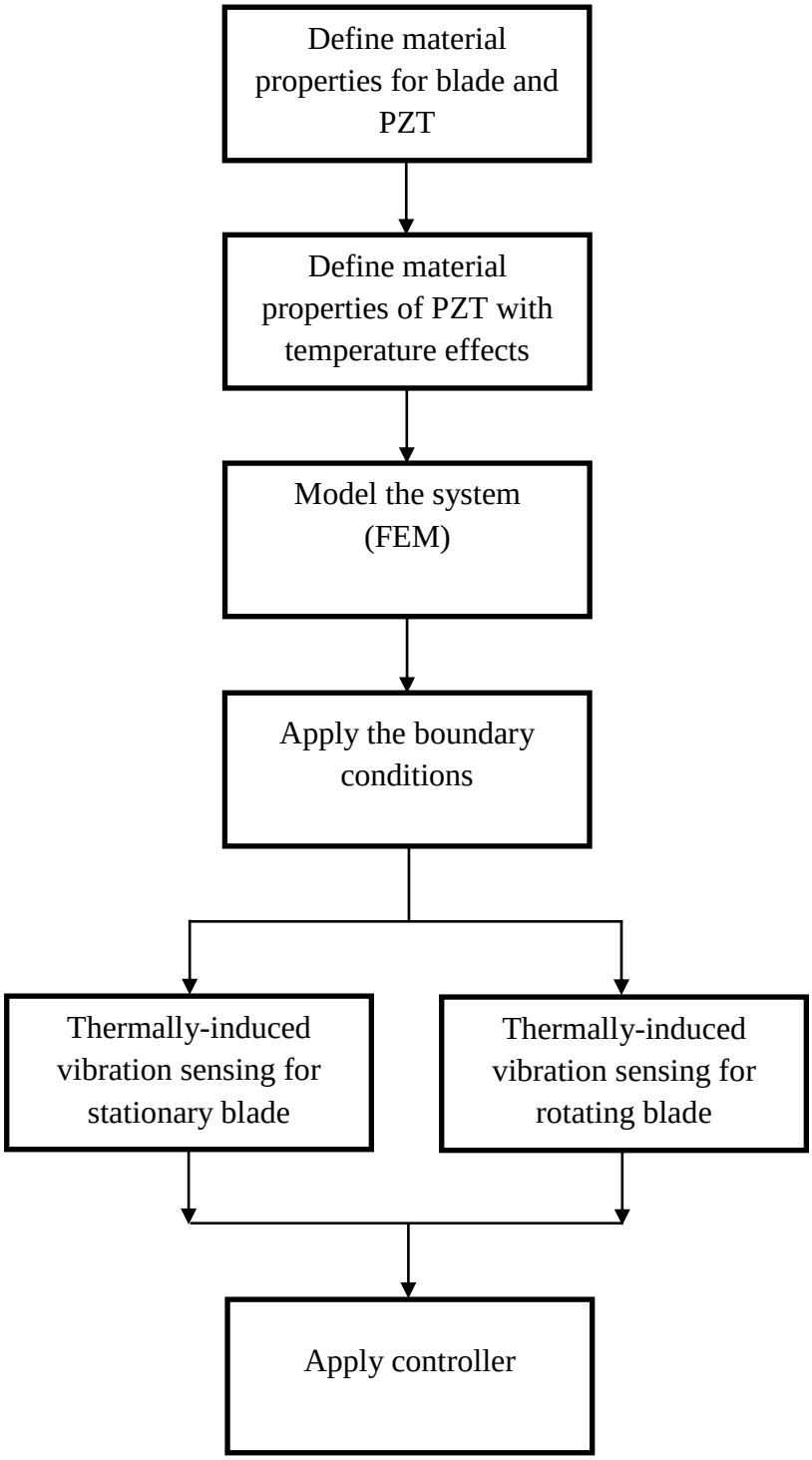

II. PROGRAM EXAMPLE

CANTILEVER BLADE WITH PZT'S

Defining material properties:

```
! Material properties for the steel blade

*SET,E,207e9                    ! Young's modulus, (N/m2)

*SET,nu,0.3                     ! Poisson's ratio

*SET,k,43                       ! Thermal conductivity, W/(m K)

*SET,rho,7800                   ! Density, kg/(m3)

*SET,alp,10.8e-6                ! Thermal expansion, (1/Celsius or 1/K)

*SET,cp,490                     ! Specific heat, (J/K)

!---------------------------------------

! Thermal properties for PZT

*SET,k_pzt,1.45                 ! PZT Thermal conductivity, W/(m K)

*SET,cp_pzt,440                 ! PZT Specific heat, (J/K)

*SET,rho,7800                   ! Density for PZT, kg/(m3)

*SET,alpx_t0,1e-6               ! PZT Thermal expansion in x direction, (1/K)

*SET,alpx_t50,1.4e-6
```

```
*SET,alpx_t100,2e-6

*SET,alpx_t150,2.7e-6

*SET,alpx_t200,3.3e-6

*SET,alpx_t250,3.9e-6

*SET,alpy_t0,1e-6              ! PZT Thermal expansion in y direction, (1/K)

*SET,alpy_t50,1.4e-6

*SET,alpy_t100,2e-6

*SET,alpy_t150,2.7e-6

*SET,alpy_t200,3.3e-6

*SET,alpy_t250,3.9e-6

*SET,alpz_t0,4e-6              ! PZT Thermal expansion in z direction, (1/K)

*SET,alpz_t50,4e-6

*SET,alpz_t100,3e-6

*SET,alpz_t150,1e-6

*SET,alpz_t200,-1.6e-6

*SET,alpz_t250,-4.2e-6

*SET,perx_t0,8.110E-9          ! Permittivity in x direction
```

```
*SET,perx_t50,9.86E-9

*SET,perx_t100,11.6E-9

*SET,perx_t150,11.9E-9

*SET,perx_t200,12.2E-9

*SET,pery_t0,8.110E-9                ! Permittivity in y direction

*SET,pery_t50,9.86E-9

*SET,pery_t100,11.6E-9

*SET,pery_t150,11.9E-9

*SET,pery_t200,12.2E-9

*SET,perz_t0,7.35E-9                 ! Permittivity in z direction

*SET,perz_t50,8.26E-9

*SET,perz_t100,9.175E-9

*SET,perz_t150,10.09E-9

*SET,perz_t200,11E-9

!---------------------------------------

! Define piezoelectric strain coefficient matrix table

tbdata,3,-5.351                      ! E31
```

```
tbdata,6,-5.351                    ! E32

tbdata,9,15.783                    ! E33

tbdata,14,12.295                   ! E16 piezoelectric constant

tbdata,16,12.295                   ! E25

!---------------------------------------

! Define piezoelectric elastic matrix (Anisotropic)

tbdata,1,120.35E9,75.18E9,75.09E9  ! D11,D12,D13

tbdata,7,120.35E9,75.09E9          ! D22,D23

tbdata,12,110.87E9                 ! D33

tbdata,16,22.57E9                  ! D44

tbdata,19,21.05E9                  ! D55

tbdata,21,21.05E9                  ! D66
```

Modeling the system (FEM):

```
*SET,l1,0.122                      ! Length of  blade

*SET,b1,0.02525                    ! Width of blade

*SET,h1,0.001                      ! Height of blade

*SET,lp,b1/2                       ! Length of PZT
```

*SET,hp,1e-3 ! Height of PZT

*SET,lp1,0.1e-3 ! Location of PZT

*SET,es,b1/10 ! Mesh size

Apply the boundary conditions:

asel,s, , , ! Fix boundary conditions for cantilever blade

asel,a, , , ! Fix boundary conditions for PZT

d,all,ux,0

d,all,uy,0

d,all,uz,0

asel,s, , , 21 ! Ground Volt PZT nodes

cp, ,volt,all

cp, ,temp,all

*get,nvA,node,0,num,min

!---------------------------------------

! Thermal loads

Tref,t0 ! Set reference temperature

q0=1e6 ! Heat flux (W/m2)

h0=10 ! Heat transfer (convection) coefficient

Applying the rotational speed:

nlgeom,on

OMEGA,,125.66,,1 ! SPINNING LOAD

OMEGA,,251.3,,1 ! SPINNING LOAD

OMEGA,,377,,1 ! SPINNING LOAD

Analysis parameters:

ts=0.15 ! Analysis time

gv=0 ! Max: 3750 for below 500 V

dss=0.001085 ! Steady state value

dt=7e-4 ! Time step

ksi1=0.01 ! Damping ratio

Applying controller:

vref=dss

veln=-(dn-dpn)/dt

va=vref-gv*((veln+…..)/n) ! Average feedback

LIST OF ABBREVIATIONS

MEMS	:	Microelectromechanical System
FGM	:	Functionally Graded Material
PID	:	Proportional Integral Derivative
FEM	:	Finite Element Method
DOF	:	Degrees of Freedom
PSD	:	Power Spectral Density

NOMENCLATURE

L	Length of the beam
b	Width of the beam
h	Height (Thickness) of the beam
T	Temperature
Q	Heat transferred (heat flux)
ρ	Material density
c	Specific heat
k	Thermal conductivity
α	Thermal expansion
E	Young's modulus (modulus of elasticity)
v	Poisson’s ratio
t	Time
τ	Nondimensional time
κ	Thermal diffusivity
A	Cross sectional area
M	Internal bending moment
M_T	Thermal moment
I	Moment of inertia
m	Nondimensional thermal moment

V	Nondimensional deflection
V_{st}	Static nondimensional deflection
v	Lateral deflection
D	Vector of electrical displacement (charge per unit area)
T	Stress vector
S	Strain vector
E	Vector of the electric field
e	Piezoelectric constant matrix
ε	Dielectric matrix at constant strain
c	Elasticity matrix at constant electric field
λ	Coefficients of thermal stress
P	Pyroelectricity
d	Matrices of coefficients of direct piezoelectric effect
η	Scalars of entropy density
g_v	Constant feedback gain matrix
ω	Angular velocity
f_n	Natural frequency
ζ	Damping ratio
∇	Gradient vector
h_c	Convective heat transfer
	Shear force

F	Load intensity
p	Thermodynamic potential
G	Energy functional
Π	Vectors of body forces
P_b	Vectors of surface forces
P_s	Vectors of concentrated forces
P_c	Electrical potential
ϕ	Surface charge
σ	Kinetic energy
Ki	

REFERENCES

[1] Sunar, M., Yilbas, B. S. and Boran, K., "Thermal and Stress Analysis of a Sheet Metal in Welding", *Journal of Materials Processing Technology*, Vol. 172, 2006, pp. 123-129.

[2] Sunar, M. and Al-Bedoor, B. O., "Vibration Measurement of a Cantilever Beam using Root Embedded pzt Sensor", *Proceedings of the Institution of Mechanical Engineers, Part C, Journal of Mechanical Engineering Science*, Vol. 222, 2008, pp. 147-161.

[3] Sunar, M. and Rao, S. S., "Recent Advances in Sensing and Control of Flexible Structures via Piezoelectric Materials Technology", *ASME Applied Mechanics Reviews*, Vol. 52, 1999, pp. 1-16.

[4] V. Giurgiutiu, "Active-Materials Induced-Strain Actuation for Aeroelastic Vibration Control", *The Shock and Vibration Digest*, Vol. 32, No. 5, 2000, pp. 355-368.

[5] Amir Manbachi, and Richard Cobbold, "Development and Application of Piezoelectric Materials for Ultrasound Generation and Detection", *Ultrasound*, Vol. 19, No. 4, 2011, pp. 187-196.

[6] Gautschi and Gustav, "Piezoelectric Sensorics: Force, Strain, Pressure, Acceleration and Acoustic Emission Sensors, Materials and Amplifiers", *Springer*, ISBN 978-3-662-04732-3, 2002.

[7] Daining Fang, Ji Wang, Weiqiu Chen, "Analysis of Piezoelectric Structures and Devices", *Physics and Astronomy Classification scheme*, 2010.

[8] World Book Encyclopedia, World Book Inc., Chicago, Vol. 15, 1992.

[9] Murozono, M., "Thermally Induced Bending Vibrations of Internally Heated Beams in Air", *Journal of Thermal Stresses*, Vol. 19, 1996, pp. 649-670.

[10] Adam, C., Heuer, R., Raue, A. and Ziegler, F., "Thermally Induced Vibrations of Composite Beams with Interlayer Slip", *Journal of Thermal Stresses*, Vol. 23, 2000, pp. 747-772.

[11] Tauchert, T. R. and Ashida, F., "Control of Thermally-Induced Structural Vibrations via Piezoelectric Pulses", *Proceedings of IUTAM Symposium on Dynamics of Advanced Materials and Smart Structures*, Yonezawa, Japan, May 20-24, 2002, K. Watanabe and F. Ziegler (Eds.), Kluwer Academic Publishers, The Netherlands, 2003, pp. 397-408.

[12] Al-Bedoor, B. and Sunar, M., "Developing a Technique for Blade Vibration Measurements in Turbomachinery & Jet Engines", *Kacst Project*, 2005.

[13] Vasques, C. M. A. and Rodrigues, J. D., "Active Vibration Control of a Smart Beam through Piezoelectric Actuation and Laser Vibrometer Sensing: Simulation, Design and Experimental Implementation", *Smart Materials & Structures*, Vol. 16, 2007, pp. 323-331.

[14] Xiang, H. J. and Yang, J., "Free and Forced Vibration of a Laminated FGM Timoshenko Beam of Variable Thickness under Heat Conduction", *Composites Part B-Engineering*, Vol. 39, 2008, pp. 292-303.

[15] Bertarelli, A., Dallocchio, A. and Kurtyka T., "Dynamic Response of Rapidly Heated Cylindrical Rods: Longitudinal and Flexural Behavior", *Journal of Applied Mechanics-Transactions of the ASME*, Vol. 75, No. 3, 2008.

[16] Suhariyono, A., Goo, N. S. and Park, H. C., "Use of Lightweight Piezo-Composite Actuators to Suppress the Free Vibration of an Aluminum Beam", *Journal of Intelligent Material Systems and Structures*, Vol. 19, 2008, pp. 101-112.

[17] Sethi, V. and Song, G., "Multimodal Vibration Control of a Flexible Structure using Piezoceramic Sensor and Actuator", *Journal of Intelligent Material Systems and Structures*, Vol. 19, 2008, pp. 573-582.

[18] U. Lee, K. Kwon, "Spectral element modeling of the thermally induced vibration of an axially moving plate", *Journal of Achievements in materials and manufacturing engineering*, Volume 26, Issue 1, January 2008.

[19] Wu, G. Y., "The Analysis of a Dynamic Instability of a Bimaterial Beam with Alternating Magnetic Fields and Thermal Loads", *Journal of Sound and Vibration*, Vol. 327, Oct 23 2009, pp. 197-210.

[20] Roy, T., Manikandan, P. and Chakraborty, D., "Development of an Improved Eight Noded Layered Shell Finite Element Formulation for Piezothermoelastic Analysis of Smart Fiber Reinforced Polymer (FRP) Composite Shell Structures with Bonded Piezoelectric Sensors and Actuators", *Finite Elements in Analysis and Design*, Vol. 46, No. 9, 2010, pp. 710-720.

[21] Narasimha Marakala, Appu Kuttan K K, Ravikiran Kadoli, "Thermally induced vibration of a simply supported beam using finite element method", *International Journal of Engineering Science and Technology*, Vol. 2(12), 2010, 7874-7879.

[22] Tauchert, T. R. and Howard, H. C., "Least-Squares Residual Solution for Displacement Control of a Composite Piezothermoelastic Cylinder", *Journal of Thermal Stresses*, Vol. 35, No. 1-3, Special Issue SI, 2012, pp. 61-74.

[23] Zhenxing Shen, Qiang Tian, Xiaoning Liu, Gengkai Hu, "Thermally induced vibrations of flexible beams using Absolute Nodal Coordinate Formulation", *Journal of Aerospace Science and Technology*, Volume 29, Issue 1, August 2013, Pages 386‑393.

[24] Jadwiga Kidawa-Kukla, "Thermally induced vibration of a cantilever beam with periodically varying intensity of a heat source", *Journal of Applied Mathematics and Computational Mechanics*, vol. 12(4), pages 59-65, 2013.

[25] Lili Gu, Zhaoye Qin, Fulei Chu, "Analytical analysis of the thermal effect on vibrations of a damped Timoshenko beam", *Journal of Mechanical Systems and Signal Processing*, November 2014.

[26] L.Malgaca, H. Al-Qahtani, M. Sunar, "Vibration Control of Rotating Blades Using Root-Embedded Piezoelectric Materiales", *Research Article - Mechanical Engineering*, Arab J Sci Eng 40:148-1495, 2015.

[27] M. Kerboua, A. Megnounif, M. Benguediab, K.H. Benrahou, F. Kaoulala, "Vibration control beam using piezoelectric-based smart materials", *Journal of Composite Structures*, Volume 123, Pages 430‑442, 2015.

[28] Mateusz Romaszko, Bogdan Sapiński, Andrzej Sioma, "Forced vibrations analysis of a cantilever beam using the vision method", *Journal of theoretical and applied mechanics*, Vol. 53, No. 1, pp. 243-254, 2015.

[29] Incropera, F. P., DeWitt, D. P., Bergman, T. L. and Lavine, A. S., *Fundamentals of Heat and Mass Transfer*, 6th Edition, Wiley, 2007.

[30] Reddy J. N., "An Introduction to the Finite Element Method", Second Edition, *Tata McGraw-Hill, New Delhi*, 2005.

[31] Stroud r. C. and Mayers J., "Dynamic Response of Rapidly Heated Plate Elements", *AIAA Journal*, 9(1), pp.76-83, 1971.

[32] Carslaw HS, Jaeger JC., "Conduction of heat in solids", Second edition, *Oxford: Clarendon Press*, 1959.

[33] Boley BA., "Thermally induced vibrations of beams", *J Aeronaut Sci*., 23:179–81, 1956.

[34] Boley, B. A. and Weiner, J. H., *Theory of Thermal Stresses*, John Wiley & Sons, 4th Printing, 1967.

[35] Ogata K., "System Dynamics", 4th Edition, Prentice-Hall, pages 395-396, 2004.

[36] Mindlin, R. D., "Equations of High Frequency Vibrations of Thermopiezoelectric Crystal Plates", *International Journal of Solids and Structures*, Vol. 10, No. 6, pp. 625-637, 1974.

[37] Tiersten H. F., "Linear Piezoelectric Plate Vibrations", *Plenum Press*, New York, 1969.

[38] Nowacki,W., "Some general theorems of thermopiezoelectricity", *J. Therm. Stress*, 1(2), l71–182, 1978.

[39] IEEE, "ANSI/ IEEE Std. 176-1987: IEEE Standard on Piezoelectricity", *The Institute of Electrical and Electronics Engineers*, New York, 1988.

[40] D. Berlincourt, H. H. A. Krueger, and C. Near, "Properties of Morgan Electro Ceramic Ceramics", *Technical Publication TP-22*, 61058-60, 1998.

[41] Sadegh Davoudi, "Effect of Temperature and Thermal Cycles on PZT Ceramic Performance in Fuel Injector Applications", *Master of Applied Science Department of Mechanical and Industrial Engineering*, University of Toronto, 2012.

[42] Bernard Jaffe, William R. Cook, Jr and Hans Jaffe, "Piezoelectric Ceramics", *Volume 3 of Non-metallic solids*, Bedford, Ohio, USA, 44146 and Cleveland, Ohio, USA, 44108, 1971.

Vitae

Name **:** AHMED SHABAN OMAR

Nationality **:** Egyptian

Date of Birth **:** 23/12/1987

Email **:** a7mad_20007@hotmail.com

Academic Background **:**

- **Master Degree of Science (M.Sc.) in Mechanical Engineering**

  King Fahd University of Petroleum & Minerals (KFUPM), June 2016.

  Dhahran, Saudi Arabia.

- **Bachelor Degree of Science (B.Sc.) in Control & Instrumentation Systems Engineering**

  King Fahd University of Petroleum & Minerals (KFUPM), June 2011.

  Dhahran, Saudi Arabia.